

Recent developments in planet migration theory

Clément Baruteau and Frédéric Masset

Abstract Planetary migration is the process by which a forming planet undergoes a drift of its semi-major axis caused by the tidal interaction with its parent protoplanetary disc. One of the key quantities to assess the migration of embedded planets is the tidal torque between the disc and planet, which has two components: the Lindblad torque and the corotation torque. We review the latest results on both torque components for planets on circular orbits, with a special emphasis on the various processes that give rise to additional, large components of the corotation torque, and those contributing to the saturation of this torque. These additional components of the corotation torque could help address the shortcomings that have recently been exposed by models of planet population syntheses. We also review recent results concerning the migration of giant planets that carve gaps in the disc (type II migration) and the migration of sub-giant planets that open partial gaps in massive discs (type III migration).

1 Introduction

The extraordinary diversity of extrasolar planetary systems has challenged our understanding of how planets form and how their orbits evolve as they form. Among the many processes contemplated thus far to account for the observed properties of extrasolar planets, the gravitational interaction between planets and their parent protoplanetary disc plays a prominent role. Considered for a long time as the key ingredient in shaping planetary systems, planet–disc interactions, which drive the

Clément Baruteau

DAMTP, University of Cambridge, Wilberforce Road, Cambridge CB30WA, United Kingdom, e-mail: C.Baruteau@damtp.cam.ac.uk

Frédéric Masset

Instituto de Ciencias Físicas, Universidad Nacional Autónoma de México (UNAM), Apdo. Postal 48-3, 62251-Cuernavaca, Morelos, México e-mail: masset@fis.unam.mx

well-known planetary migration (a drift of a planet's semi-major axis during the lifetime of the gaseous disc), have recently been considered by many as being over-emphasized. On the one hand, observational data show evidence for vigorous migration in many planetary systems, as stressed by the existence of hot Jupiters, Neptunes and Super-Earths (the recently discovered Kepler-20 planetary system, with coplanar rocky and icy planets alternating at periods less than 80 days [30], provides a good example), or by the existence of many mean-motion resonances. Yet, there is also compelling evidence that other processes are capable of altering the orbits as dramatically as planet–disc interactions (the existence of highly-eccentric or retrograde planets is an example). Also, although many systems seem to have undergone orbital migration, many others display planets at distances from their star that are of same order of magnitude as the distances of the planets in our Solar System to the Sun. One may be tempted to conclude from this that theories of planet–disc interactions are overrated, to the point that they could be merely ignored in scenarios of formation of planetary systems. Yet, as will be detailed in the following sections, the following facts are difficult to circumvent:

- Each component of the torque exerted by the disc on a planet is so large that it can half or double the planet's semi-major axis in a time that is usually two or more orders of magnitude shorter than the lifetime of protoplanetary discs.
- These torque components do not cancel out. The residual torque amounts to a fair fraction of each torque component, so that one should in general expect that planet–disc interactions have a strong effect on planets orbits over the disc lifetime.

The central difficulty in planetary migration theories lies precisely in predicting the residual torque value. In addition to being a fair difference between several large amplitude torques, it is very sensitive to the disc properties near the planet's orbit (e.g., density, temperature profiles). This by no means implies that the total torque is negligible, but it helps understand why migration theories are slowly maturing.

One of the main purposes of this review is to provide the reader with an up-to-date presentation of the state of planet–disc interactions, with emphasis on the torque formulae that govern the migration of low-mass planets. The reasons for this special emphasis are three-fold:

- Low-mass planets are the most critical in planetary population synthesis, as they potentially undergo the fastest migration.
- The sensitivity of detection methods has increased to a point where we can find a plethora of Neptune-sized planets or below, which exclusively underwent the migration processes typical of low-mass planets during their formation.
- The subject has been the focus of significant efforts in the recent past.

The torque acting on a low-mass planet in circular orbit can be decomposed into two components: (i) the differential Lindblad torque, arising from material passing by the planet at supersonic velocities, which is deflected by the latter and therefore exchanges angular momentum and energy with the planet, and (ii) the corotation torque, arising from material slowly drifting with respect to the planet, in the vicinity of its orbit. The differential Lindblad torque has been extensively studied from

the early times of planetary migration theories, and is known in much greater detail than the corotation torque. In fact the corotation region, which has been under intense scrutiny over the last five years, has proved to have a much more complex dynamics than previously thought. In particular, the value of the corotation torque depends sensitively on the radiative properties of the gas disc, and may exhibit large values when the gas is radiatively inefficient (as is generally expected in regions of planet formation). In addition to this complexity, new problems emerge as the computational resources render tractable the task of simulating a planet embedded in realistic discs, namely three-dimensional discs invaded by turbulence.

This review is organised as follows. After a brief description of the physical model and notations in § 2, we present in § 3 the migration of low-mass planets (type I migration). We detail some recent results on the differential Lindblad torque in § 3.1, and we put special emphasis on the recent developments on the corotation torque in § 3.2. The migration of gap-opening planets is then examined in § 4, with type III migration in § 4.2, followed by type II migration in § 4.3. Finally, in section § 5, we discuss some recent themes related to planet–disc interactions, such as the discovery of massive planets at large orbital separations, and recent models of planetary population syntheses. Most sections end with a brief summary of their content.

2 Physical model and notations

In most of the following we shall consider two-dimensional discs, considering vertically averaged or vertically integrated quantities where appropriate. At the present time, most of the recent investigation on the migration of low-mass planets has been undertaken in two dimensions (with a list of exceptions that includes, but is not restricted to [102, 22, 23, 12, 111, 86, 87, 43, 3]), and much insight can be gained into the mechanisms of the different components of the torque exerted by the disc on the planet through a two-dimensional analysis. It should be remembered, however, that two-dimensional results are plagued by the unavoidable use of a softening length for the planet’s gravitational potential, which fits a two-fold purpose:

- It mimics the effects of the finite thickness of a true disc, by lowering the magnitude of the planet’s potential well.
- In numerical simulations, it avoids the potential divergence at the scale of the mesh zone.

For this reason, the reader should bear in mind that the ultimate torque expressions should be sought by means of three-dimensional calculations, and that two-dimensional calculations are only used in a first step to elucidate the mechanisms that contribute to the torque. At the time of writing this manuscript, most of the physics of the torque in two dimensions is fairly well understood, which is why we put special emphasis on the two-dimensional analysis.

We consider a planet of mass M_p orbiting a star of mass M_* with orbital frequency Ω_p . We denote by q the planet-to-primary mass ratio. The planet is assumed to be on a prograde circular orbit of semi-major axis a , coplanar with the disc, so that we do not consider in this work eccentric, inclined, or retrograde planets. The protoplanetary disc in which the planet is embedded is modelled as a two-dimensional viscous disc in radial equilibrium, with the centrifugal acceleration and the radial acceleration related to the pressure gradient balancing the gravitational acceleration due to the central star. We use P to denote the vertically integrated pressure, and s to denote (a measure of) the gas entropy, which we express as

$$s = \frac{P}{\Sigma\gamma}, \quad (1)$$

where Σ is the surface density of the gas and γ the ratio of specific heats C_p/C_v . We denote with T the vertically averaged temperature. We assume in most of what follows that the surface density and temperature profiles are power laws of radius, with indices α and β , respectively:

$$\Sigma \propto r^{-\alpha} \quad (2)$$

and

$$T \propto r^{-\beta}. \quad (3)$$

The disc pressure scale length is $H = c_s/\Omega$, with Ω the gas orbital frequency and c_s the sound speed. We define the disc aspect ratio by $h = H/r$. When T is a power law of radius, so is h , with an index f dubbed the flaring index:

$$h \propto r^f, \quad (4)$$

which satisfies $\beta = 1 - 2f$. In almost all studies of planet–disc interactions, the disc is modelled with a stationary kinematic viscosity ν , aimed at modelling the disc’s turbulent properties. We will consider that ν can be written as $\nu = \alpha_v H^2 \Omega$ [100], with α_v denoting the alpha viscous parameter associated with the turbulent stresses in the disc.

We will also make use of Oort’s constants. The first Oort’s constant scales with the shear of the flow,

$$A = \frac{1}{2} r \frac{d\Omega}{dr}, \quad (5)$$

while the second Oort’s constant scales with the vertical component of the vorticity of the flow ω_z :

$$B = \frac{1}{2r} \frac{d(r^2\Omega)}{dr} = \frac{\omega_z}{2}. \quad (6)$$

Whenever used, A and B are implicitly meant to be evaluated at the planet’s orbital radius.

The governing equations of the flow are the equation of continuity, the Navier-Stokes equations and the energy equation (except when dealing with isothermal

discs, as specified below), together with the closure relationship provided by the equation of state, which is that of an ideal gas. We do not reproduce these governing equations here, but refer the interested reader to, for example, [68, 14, 84, 19, 23, 21].

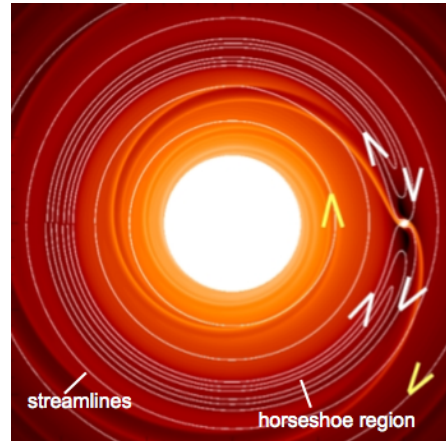
3 Migration of low-mass embedded planets: Type I migration

Up until recently, type I migration referred to the regime of migration of low-mass planets that could be tackled through a linear analysis [46, 102]. Recently, however, [89] have shown that one of the torque components, namely the corotation torque, can become non-linear at all planetary masses, provided the disc viscosity is sufficiently small. We shall nevertheless still qualify type I as the migration of low-mass planets, up to a threshold mass that we shall specify in § 4.1. We entertain below the two components of the tidal torque: the differential Lindblad torque and the corotation torque. In the following, we address the properties of type I migration by a direct inspection of the tidal torque Γ , where the planet migration rate \dot{a} is given by

$$2Ba\dot{a}M_p = \Gamma. \quad (7)$$

3.1 Differential Lindblad torque

Fig. 1 Disc's surface density perturbed by a low-mass planet. Streamlines in the frame corotating with the planet are overplotted by solid curves. The set of streamlines that librate with respect to the planet delimits the planet's horseshoe region.



The differential Lindblad torque accounts for the exchange of angular momentum between the planet and the trailing density waves (spiral wakes) that it generates in the disc (see illustration in Fig. 1). The density waves propagating inside the planet's

orbit carry away negative angular momentum, and thus exert a positive torque on the planet, named the inner Lindblad torque. Similarly, the spiral density waves propagating outside the planet's orbit carry away positive angular momentum, which corresponds to a negative torque on the planet (the outer Lindblad torque). The angular momentum of a planet on a circular orbit scales with the square root of its semi-major axis. The inner Lindblad torque thus tends to make the planet move outwards, while the outer Lindblad torque tends to make it move inwards. The residual torque, called differential Lindblad torque, results from a balance between the inner and outer torques. In the absence of viscosity, the angular momentum taken away by the wakes is conserved until wave breaking occurs, resulting in the formation of a shock and the deposition of the wave's energy and angular momentum to the disc [33]. The impact of non-linearities induced by the planet's wakes, which in particular lead to the formation of a gap about the planet's orbit, will be described in Section 4.1.

The one-sided and differential Lindblad torques can be evaluated in different manners:

1. In a fully analytic manner upon linearization of the flow equations [31]. In this framework, waves propagate away from Lindblad resonances with the planet [106], and they constructively interfere into a one-armed spiral pattern [83], which begins where the Keplerian flow is supersonic with respect to the planet [33]. One-sided Lindblad torques are then evaluated as the sum of the torques arising at each Lindblad resonance. The locations of Lindblad resonances are shifted with respect to their nominal location (given by the condition of mean-motion resonance with a test particle) by pressure effects. In particular, resonances with high azimuthal wavenumber have accumulation points at $\pm 2H/3$ from the planetary orbit, instead of accumulation at the orbit. This provides a torque cutoff [32, 2], which can only be evaluated approximately [1]. This renders fully analytic methods of Lindblad torque calculations only approximate.
2. The torque can be evaluated by solving numerically the linearised equations of the flow. This approach was initially undertaken by [46], and recently revisited by [88] and [84].
3. An intermediate approach may be used, in which one solves numerically linear equations obtained by an expansion of the flow equations in H/r , where H is the disc thickness [102].

Fig. 2 illustrates a number of properties of the Lindblad torque that provide some insight into its scaling with the disc and planet parameters. In this figure, the torque value has been obtained through the use of analytical formulae similar to that of [108] (Eqs. 3 to 7 therein), except for the introduction of a softening length for the planet's potential, and for the minor correction consisting of the introduction of a factor Ω/κ in the forcing terms (see [74], after their Eq. 13; κ denotes the horizontal epicyclic frequency). This figure shows that the torque undergoes a sharp cutoff past a peak value, which is found to be of order $m_{\max} \sim (2/3)(r/H)$. Also, the dashed line shows that, up to the cutoff, the one-sided Lindblad torque approximately scales with m^2 – as expected from the WKB analysis of [32] – from which we infer the

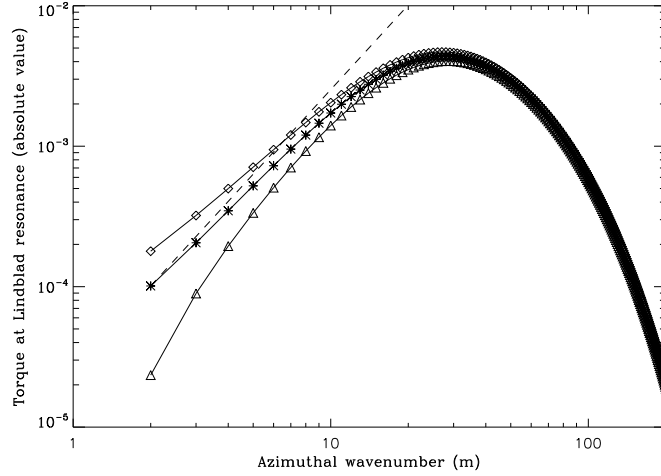


Fig. 2 Torques at individual outer Lindblad resonances (diamonds) and inner Lindblad resonances (triangles), in absolute value. Results are obtained for a disc with aspect ratio $H/r = 0.02$, and with a softening length $\varepsilon = 0.5H$ for the planet potential. Torques are normalised to the torque value given by Eq. (8). Stars show the average value of the inner and outer Lindblad torques at a given azimuthal wavenumber m , and the dashed line illustrates its m^2 dependence at small m .

one-sided Lindblad torque, summed over m , to scale approximately as m_{\max}^3 , *i. e.* as $(r/H)^3$. Besides, the torque naturally scales with the disc's surface density and with the square of the planet mass, and dimensional arguments further imply that it ought to scale as:

$$\Gamma_0 = \Sigma q^2 \Omega^2 a^4 / h^3, \quad (8)$$

which is indeed the scaling of the one-sided Lindblad torque [108].

Fig. 2 also shows that there exists an asymmetry between the outer and inner torques, the former being systematically larger than the latter. The reasons for this asymmetry are examined in depth in [108]. The relative asymmetry is found to scale with the disc thickness: in thinner discs, the relative asymmetry of the inner and outer torque is smaller (which can be understood as due to the accumulation points of the inner and outer resonances lying closer to the orbit). As a consequence, the differential Lindblad torque scales with:

$$\Gamma_{\text{ref}} = \Sigma q^2 \Omega^2 a^4 / h^2. \quad (9)$$

The asymmetry between the inner and outer torques also depends upon:

- The temperature gradient, since it affects the location of Lindblad resonances, and therefore the magnitude of the forcing potential at a given resonance [106]. For instance, a steeper (decreasing) temperature profile decreases the disc's angular frequency (by increasing the magnitude of the radial pressure gradient), which shifts all Lindblad resonances inwards. Outer resonances get closer to the

planet orbit, which strengthens the outer torque, whereas inner Lindblad resonances are shifted away from the planet orbit, which decreases the inner torque. The net effect of a steeper temperature gradient is therefore to make the differential Lindblad torque a more negative quantity. In the same vein, a shallower temperature gradient would shift all Lindblad resonances outwards, making the differential Lindblad torque a more positive quantity. The differential Lindblad torque may become positive for positive temperature gradients [108].

- The surface density gradient, which affects the location of Lindblad resonances in the exact same way as the temperature gradient, but now also because the torque at a given Lindblad resonance directly scales with the underlying surface density [106]. A steeper (decreasing) density profile naturally increases the magnitude of the inner torque compared to that of the outer torque, but this effect is mostly compensated for by an inward shift of all Lindblad resonances (just like when steepening the temperature profile, as described above). It implies that the differential Lindblad torque is quite insensitive to the density gradient near the planet location.
- The disc's self-gravity, which also impacts the location of Lindblad resonances, essentially by changing the wave's dispersion relation [96, 10].

An accurate determination of the asymmetry between the inner and outer torques yields a dimensionless factor to be put in front of Γ_{ref} to give the expression for the differential Lindblad torque. This issue has triggered a lot of theoretical efforts in the last three decades, and it is not completely solved yet. As of the writing of this review, the two main results are:

- An expression obtained by solving numerically the linearised equations of the flow in two dimensions with a softened planet potential, in discs with arbitrary gradients of surface density and temperature [88, 84]. It takes the form:

$$\frac{\Gamma_L}{\Gamma_{\text{ref}}} = -(2.5 + 1.7\beta - 0.1\alpha) \left(\frac{0.4}{\varepsilon/H} \right)^{0.71}, \quad (10)$$

with α and β defined in Eqs. (2) and (3). The expression in Eq. (10) is most accurate for softening lengths $\varepsilon \sim 0.4H$.

- An expression obtained by a semi-analytic method for globally isothermal, three-dimensional discs with arbitrary gradients of surface density [102]:

$$\frac{\Gamma_L}{\Gamma_{\text{ref}}} = -(2.34 - 0.10\alpha). \quad (11)$$

We note that Eqs. (10) and (11) exhibit a similar behaviour (for the case $\beta = 0$, exclusively contemplated by [102]), that is to say a constant term of similar magnitude, and a weak dependence on the surface density gradient. Yet, the latter depends strongly on the softening length, as can be noticed by comparing to the two-dimensional, unsmoothed, globally isothermal expression also provided by [102]:

$$\frac{\Gamma_L}{\Gamma_{\text{ref}}} = -(3.20 + 1.47\alpha). \quad (12)$$

This raises the question of whether the dependence on the temperature gradient, in a three-dimensional disc, would be as steep as that of Eq. (10). Thus far this is an unanswered question, even if recent numerical simulations seem to indicate that the dependence of the differential Lindblad torque on the temperature gradient in a three-dimensional disc is comparable to that of a two-dimensional disc with a smoothing length $\varepsilon \simeq 0.4H$ (Casoli & Masset, in prep). We also comment that self-gravity slightly enhances the amplitude of the differential Lindblad torque by a factor approximately equal to $(1 + Q_p^{-1})$, with Q_p the Toomre Q-parameter at the planet's orbital radius [10].

Unless the disc has a temperature profile that strongly increases outward, the differential Lindblad torque is a negative quantity which, by itself, would drive type I migration on timescales shorter than a few $\times 10^5$ yrs for an Earth-mass object in a disc with a mass comparable to that of the Minimum Mass Solar Nebula [108]. Note however that Eqs. (10) and (11) have been derived under the assumption that the profiles of surface density and temperature are power laws of the radius. Local variations in the disc's temperature and/or density profiles, due for example to opacity transitions [74] or to dust heating [34] may change the sign and magnitude of the differential Lindblad torque. An approximate generalisation of the Lindblad torque expression, valid in non-power law discs, has been derived by [67] for two-dimensional discs with a softening length $\varepsilon = 0.6H$. This expression reads:

$$\frac{\Gamma_L}{\Gamma_{\text{ref}}} = -(2.00 - 0.16\alpha + 1.11\beta - 0.80[\beta_2^+ - \beta_2^-]), \quad (13)$$

where

$$\beta_2 = h \frac{d^2 \log T}{d(\log r)^2}, \quad (14)$$

and where a quantity with a \pm subscript is to be evaluated in $r = a \pm H/5$. Obviously, if the temperature profile is a power-law of radius, one has $\beta_2^+ = \beta_2^- = 0$, and Eq. (13) reduces to a standard linear combination of α and β .

The differential Lindblad torque has also been investigated in strongly magnetised, non-turbulent discs. The case of a two-dimensional disc with a toroidal magnetic field has been studied by [103] through a linear analysis. She found that the differential Lindblad torque is reduced with respect to non-magnetised discs (as waves propagate outside the Lindblad resonances at the magneto-sonic speed $(c_s^2 + v_A^2)^{1/2}$, with v_A the Alfvén speed, rather than the sound speed c_s). Additional angular momentum is taken away from the planet by the propagation of slow MHD waves in a narrow annulus near magnetic resonances. These results were essentially confirmed by [28] with non-linear 2D MHD simulations in the regime of strong toroidal field (the plasma β -parameter, $\beta = c_s^2/v_A^2$, was taken equal to 2 in their study). More recently, 2D and 3D disc models with a poloidal magnetic field were investigated by [79] with a linear analysis in the shearing sheet approximation. While the differential Lindblad torque is reduced similarly as with a toroidal magnetic field, extraction

of angular momentum by slow MHD and Alfvén waves is found to occur in three dimensions only.

We sum up the results presented in this section.

- The differential Lindblad torque corresponds to the net rate of angular momentum carried away by density waves (wakes) the planet generates in the disc at Lindblad resonances.
- The sign and magnitude of the differential Lindblad torque arise from a slight asymmetry in the perturbed density distribution associated to each wake.
- The differential Lindblad torque is a stationary quantity, largely independent of the disc's turbulent viscosity. Alone, it would drive the migration of Earth mass embedded planets in as short a time as a few $\times 10^5$ yrs in typical protoplanetary discs.

3.2 Corotation torque

The other component of the tidal torque, the corotation torque, has long been neglected in studies of planetary migration. Firstly, it was shown to have a lower absolute value than the differential Lindblad torque for typical (decreasing) radial profiles of the disc's surface density [102]. Secondly, this torque component, for reasons that will be presented at length in section 3.3, should tend to zero after a finite time in an inviscid disc (the corotation torque is said to "saturate"). However, as indicated by [107], some amount of turbulence should prevent the corotation torque from saturating, and in the last decade the asymptotic value of the torque at large time in the presence of dissipative processes has been tackled either analytically [64, 5], by means of numerical simulations [65], or both [69, 85]. Besides, it was discovered by [86] that in radiative discs, the corotation torque could, under certain circumstances, be so large and positive that it could largely counteract the differential Lindblad torque, thereby leading to outward planetary migration. This was subsequently interpreted as a new component of the corotation torque arising from the disc's entropy gradient [9, 88, 68, 84].

The corotation torque on low-mass planets is usually linked to the so-called horseshoe drag, which corresponds to the exchange of angular momentum between the planet and its horseshoe region. The planet's horseshoe region encompasses the disc region where fluid elements are on horseshoe streamlines with respect to the planet orbit (see Fig. 1). We therefore start by explaining the concept of horseshoe dynamics and horseshoe drag.

3.2.1 Horseshoe dynamics

In the restricted three-body problem (RTBP), it is useful to write the Hamiltonian of the test particle in the frame that corotates with the secondary. In this frame, the potential does not depend explicitly on time and the Hamiltonian H is therefore

conserved. It reads:

$$H = E - \Omega_p L, \quad (15)$$

where E is the total energy of the test particle as seen in an inertial frame centred on the primary, and L its angular momentum. The Hamiltonian of Eq. (15) is usually called the Jacobi constant. A sketch of the lines of constant Jacobi value when the kinetic energy is zero (E therefore exclusively amounts to the potential energy), named zero velocity curves (ZVC), reveals the existence of a horseshoe-like region encompassing the secondary's orbit [78]. Furthermore, in the limit of a small secondary's mass, the trajectory of the guiding centre of the test particle in this area is shown to have a radial displacement from the orbit that is twice that of the associated ZVC [78], so that the guiding centre of a test particle can also exhibit a horseshoe-like motion in the vicinity of the orbit. In a similar fashion, a gas parcel in a disc with pressure can exhibit a horseshoe-like motion, very similar to that of the RTBP. There are, however, important differences between these two cases. Firstly, in the RTBP, the test particle can exhibit epicyclic motion on top of its global horseshoe-like trajectory. In the horseshoe region of a low mass planet, where no shocks are present, the gas parcels cannot cross each other's orbits, and therefore essentially follow nearly circular streamlines far from the planet. Secondly, the width of the horseshoe region is quite different in the two cases. It is much more narrow, for the same planetary mass, in the gaseous case than in the RTBP. Also, it has a different scaling with the planetary mass in the two cases: in the RTBP, the width of the horseshoe region scales with the cube root of the planetary mass, whereas in the gaseous case, provided the planet mass is not too large (we will specify how large below), it scales with the square root of the planet mass. To understand the reasons for this difference, we depict in the left-hand panel of Fig. 3 the streamlines in the vicinity of the coorbital region of a low-mass planet. The planet is located at radius $r = 1$,

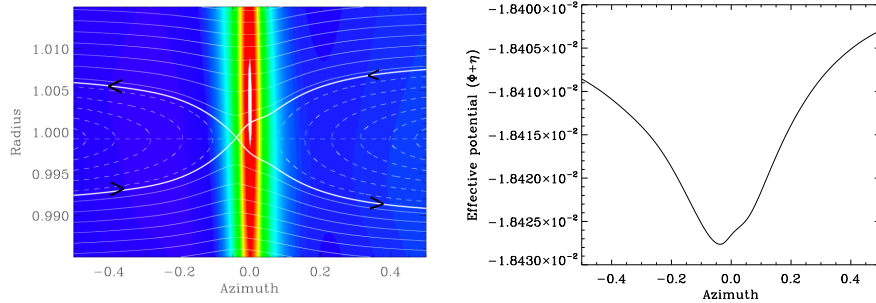


Fig. 3 Left: streamlines in the vicinity of an Earth-mass planet embedded in a disc with $H/r = 0.05$. The softening length of the potential is $\epsilon = 0.6H$. The thick lines show the separatrices of the horseshoe region (the frontiers between the dashed streamlines that exhibit horseshoe-like motion and the solid ones corresponding to circulating material with respect to the planet orbit). A few arrows show the flow's direction with respect to the planet. The horizontal dashed line shows the corotation radius, where the angular velocities of the disc and the planet are equal. Right: effective potential at the corotation radius, as a function of azimuth.

and azimuth $\varphi = 0$. The separatrices of the planet's horseshoe region are depicted by thick curves. We see that, quite to the contrary of the RTBP, there is no equivalent to the Roche lobe region around the planet (no circulating fluid material bound to it). Another difference is that the fixed point (or stagnation point) at which the separatrices intersect lies on the orbit (whereas in the RTBP, they intersect at the Lagrange points, away from the orbit, on a line joining the central star and the planet [78]). The azimuth of the stagnation point corresponds to the azimuth where, at corotation, the effective potential (the sum of the gravitational potential and fluid enthalpy) is minimum. This is illustrated in the right panel of Fig. 3. The sign and value of the stagnation point's azimuth is closely related to the asymmetry of the inner and outer wakes generated by the planet [90]. Note that there may be several stagnation points near the planet's corotation radius, depending on the softening length of the planet's potential [14].

Assuming that the fluid motion is in a steady state in the vicinity of the planet, we may use a Bernoulli invariant in the corotating frame [72, 70, 14]. This invariant can be cast as:

$$B_J = \frac{v^2}{2} + \eta + \Phi - \frac{1}{2}r^2\Omega_p^2, \quad (16)$$

where v is the fluid velocity in the corotating frame, η the fluid's specific enthalpy, Φ the sum of the star's and the planet's gravitational potentials, and Ω_p the planet's angular frequency. Equating the value of the Bernoulli invariant at the stagnation point (where by definition $v = 0$), and far from the planet on a separatrix, one finds the following expression for the half-width x_s of the planet's horseshoe region, away from the planet:

$$x_s \propto |\Phi_p + \eta'|_s^{1/2}, \quad (17)$$

where Φ_p is the planetary potential and η' the perturbation of the gas specific enthalpy introduced by the planet. The s subscript on the right hand side of Eq. (17) means that these variables are to be evaluated at the stagnation point. When the planet mass is sufficiently small, the streamlines are found to be in good agreement with those inferred from the linear expansion of the perturbed velocity field. Note that this does not imply that the corotation torque is in general a linear process. As was shown indeed by [89], the torque exerted by the coorbital material on the planet eventually becomes non-linear, no matter how small the planet mass is, provided dissipative effects are sufficiently small. However, the fact that important non-linear processes take place in this region hardly affects the streamlines themselves. In this low-mass regime, the stagnation point has therefore a location independent of the planet mass, necessarily at the corotation radius. In that case, the effective perturbed potential $\Phi_p + \eta'$ scales with the planet mass (M_p), and Eq. (17) implies that $x_s \propto M_p^{1/2}$. This is no longer true when the location of the stagnation point depends on the planet mass. In particular, in the high-mass regime, the planet gravity dominates over the perturbed enthalpy, and the situation resembles that of the RTBP. The Bernoulli invariant at the inner and outer stagnation points (which are L₁-like and L₂-like, respectively) is dominated by the planetary potential term and so scales as M_p/R_H , where $R_H = a(M_p/M_\star)^{1/3}$ is the planet's Hill radius. In the high-mass

region, the width of the horseshoe region therefore scales with the cubic root of the planet mass, as in the RTBP [70].

Lastly, another important difference between the RTBP and the case of a low-mass embedded planet is that of the U-turn timescale. Firstly, it should be noted that the expression *U-turn timescale* is ambiguous, for it depends on the horseshoe streamline under consideration. The closer to corotation, the longer it takes to perform a horseshoe U-turn, and the U-turn time reaches its minimum value close to the separatrix. It is usually this minimum value that is meant by the ambiguous expression *U-turn timescale*. Note that the corotation torque nearly reaches a constant value (notwithstanding saturation considerations, that we shall contemplate later) after this timescale, as it corresponds to the fluid elements that most contribute to the torque, because their angular momentum jump is the largest, and because their mass flow-rate is large.

In the RTBP, the U-turn timescale is of the order of the dynamical timescale τ_{dyn} , *i.e.* a planet orbital period. If one regards, in a crude approximation, the case of a low-mass embedded planet as an expurgated version of the RTBP, where most of the initial horseshoe streamlines are made circulating, and where only those lying close to corotation keep their horseshoe character, one expects the U-turn timescale in this case to be significantly longer than the dynamical timescale. This is indeed the case: the U-turn timescale is approximately $h_p \tau_{\text{lib}}$ [9], with h_p the disc's aspect ratio at the planet's orbital radius, and where τ_{lib} is the libration timescale, *i.e.* the time it takes to complete a closed horseshoe trajectory. The libration timescale reads

$$\tau_{\text{lib}} = \frac{8\pi a}{3\Omega_p x_s}. \quad (18)$$

An alternate, equivalent expression for the U-turn timescale is $\tau_{\text{U-turn}} \sim \tau_{\text{dyn}} H/x_s$, which is corroborated by numerical simulations in which one monitors the advection of a passive scalar. This expression shows that the U-turn timescale can indeed be longer than the dynamical timescale by a significant factor, as x_s can be much smaller than H for deeply embedded, low-mass objects.

We sum up the results presented in this section:

- The coorbital region of a low-mass embedded planet in a gaseous disc exhibits a horseshoe-like region.
- This region is much more narrow than in the restricted three-body problem, and its radial width scales with the square root of the planetary mass.
- The stagnation points are located at the corotation radius. There is no equivalent to the Roche lobe region for low-mass objects.
- The horseshoe U-turn timescale is significantly longer than the dynamical timescale.

3.2.2 Horseshoe drag: an overview

Far from the horseshoe U-turns in the vicinity of the planet, a fluid element or test particle essentially follows a nearly circular orbit, and therefore has a nearly constant

angular momentum. When it reaches a U-turn, a fluid element is either sent inward or outward, thereby crossing the planet orbit. It does so by exchanging angular momentum and energy with the planet. The torque resulting from the interaction of the planet with all the fluid elements in the course of performing their horseshoe U-turn is called horseshoe drag [107].

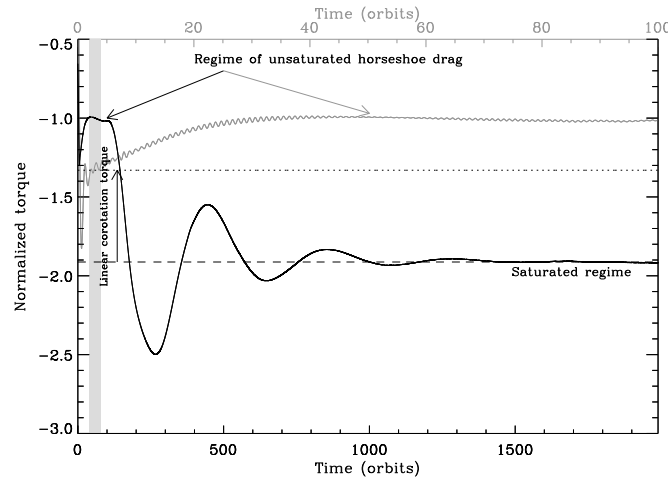


Fig. 4 Time evolution of the total torque (sum of the differential Lindblad torque and corotation torque) on a $M_p = 10^{-6}M_*$ planet mass embedded in an inviscid isothermal disc. The black curve (bottom x-axis) shows the torque evolution over 2000 planet orbits, while the grey curve (top x-axis) focuses on the evolution over the first 100 planet orbits. The dashed line shows the value of the differential Lindblad torque, and the dotted curve highlights the corotation torque predicted with a linear analysis. Taken from [67].

Upon insertion of the planet in the disc, it takes some time to establish the horseshoe drag, namely a time of the order of the horseshoe U-turn timescale [89]. This is illustrated in Fig. 4, which displays the time evolution of the total torque on a $M_p = 10^{-6}M_*$ mass planet embedded in a thin ($h = 0.05$) isothermal disc with uniform density profile. The disc is inviscid in this example. Once established (after ~ 30 planet orbits in our example), the horseshoe drag remains approximately constant over a longer timescale, which corresponds to the time it takes for a fluid element to drift from one end of the horseshoe to the other (that is, about half a libration time, given by Eq. (18)). The value of the horseshoe drag that exists between the horseshoe U-turn time, and half the horseshoe libration time, is called the *unsaturated horseshoe drag*. Beyond this stage, subsequent U-turns may cause further time evolution of the horseshoe drag depending on the disc viscosity, which will be described in § 3.3. In the particular case depicted here, where the disc is inviscid, the horseshoe drag eventually saturates (it cancels out) after a few libration timescales. Until § 3.3, we focus on the properties of the fully unsaturated horseshoe drag.

3.2.3 Horseshoe drag in barotropic discs

A hint of the torque exerted by the coorbital material on the planet can be obtained by the examination of the perturbed surface density. Nonetheless, this examination is rather difficult, because the density perturbation in the planet's coorbital region is very small, typically one or two orders of magnitude smaller than the density perturbation associated to the wakes. Yet, as can be seen in Fig. 5, an approximate subtraction of the wakes density perturbation reveals two regions of opposite signs: a region of positive perturbed density ahead of the planet ($\phi > 0$) and a region of negative perturbed density behind the planet ($\phi < 0$), which both yield a positive torque on the planet. The sign of the perturbed density in the coorbital region depends on the background density profile, here it is uniform ($\alpha = 0$). The largest perturbations can be seen to originate near the downstream separatrix in either case (the outer separatrix at negative azimuth, and the inner separatrix at positive azimuth), but the perturbation is spread radially and extends much beyond the horseshoe region. This is to be expected on general grounds: in a barotropic disc, where the gas pressure depends only on its mass density, any disturbance near corotation excites evanescent pressure waves, which extend typically over the disc pressure length scale (here $H = 0.05a$).

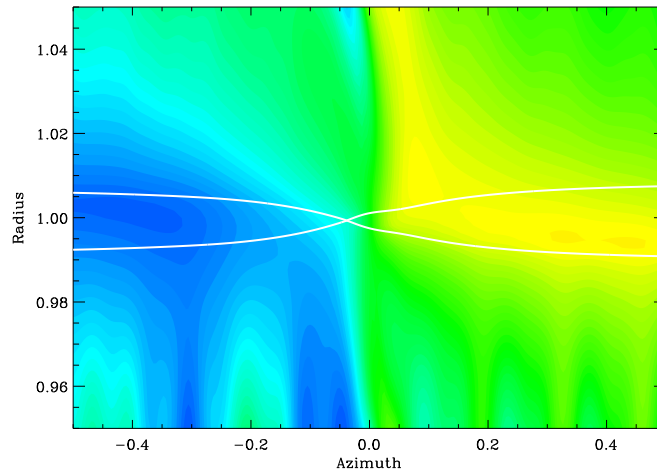


Fig. 5 Perturbed surface density in the coorbital region of an Earth-mass planet in a disc with $h = 0.05$ and $\alpha = 0$ (uniform background surface density). The planet is located at $r = 1$, $\varphi = 0$. The solid curves show the separatrices of the planet's horseshoe region. In order to remove the planet's wakes and to render this map more legible, we have subtracted the density perturbation obtained in a situation where no corotation torque is expected (namely $\alpha = 3/2$, as will be shown below). This cancellation is imperfect, however, as the wakes of the two cases are not strictly identical.

Even if some insight into the corotation torque can be gained by the examination of the perturbed density maps, a much more useful quantity is the vortensity (the ratio of the vertical component of the vorticity to the surface density, also known as potential vorticity), which is materially conserved away from shocks in inviscid, barotropic, two-dimensional discs. This is illustrated in Fig. 6. [107] has evaluated

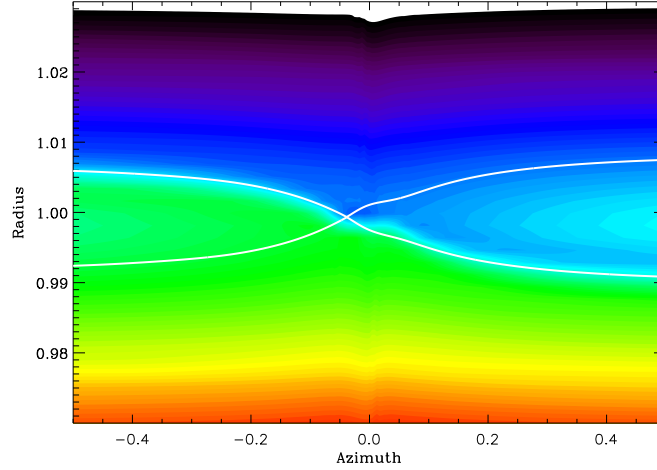


Fig. 6 Advection of vortensity in the horseshoe region of an embedded, low-mass protoplanet. As in previous panels, the planet is at $r = 1$, $\varphi = 0$, and the separatrices of the planet's horseshoe region are depicted by white curves. The unperturbed disc's vortensity decreases with radius. The (high) vortensity in the inner side of the horseshoe region (at $\varphi < 0$, $r < 1$) is brought to the outer side (at $\varphi < 0$, $r > 1$) by the outward U-turns behind the planet. Similarly, the (low) vortensity in the outer side of the horseshoe region (at $\varphi > 0$, $r > 1$) is brought to the inner side (at $\varphi > 0$, $r < 1$) by the inward U-turns ahead of the planet.

the torque exerted on the planet by test particles embarked on horseshoe motion, by making use of the Jacobi invariant of these particles (see section 3.2.1). A similar calculation can be performed for fluid motion, provided one uses a Bernoulli invariant by adding the enthalpy to the Jacobi constant [72, 14]. In both cases one finds that the horseshoe drag has the following expression:

$$\Gamma_{\text{HS}} = 8|A|B^2a \left[\int_{-x_s}^{x_s} \left(\left. \frac{\Sigma}{\omega_z} \right|_F - \left. \frac{\Sigma}{\omega_z} \right|_R \right) x^2 dx \right], \quad (19)$$

where x denotes the radial distance to the planet orbit. In Eq. (19), the subscript F indicates that the (inverse of) the vortensity Σ/ω_z has to be evaluated away from the planet, in Front of the latter ($\phi > 0$), and the subscript R indicates that it has to be evaluated at the Rear of the planet, away from it ($\phi < 0$). The integral in Eq. (19) is usually called the horseshoe drag integral, and in a barotropic disc it can be simplified to yield the following expression [14, 84, 69]:

$$\Gamma_{\text{HS}} = \frac{3}{4} \Sigma \mathcal{V} \Omega_p^2 x_s^4, \quad (20)$$

where the quantity \mathcal{V} , called the (inverse) vortensity gradient for short, is defined by

$$\mathcal{V} = \frac{d \log(\Sigma/B)}{d \log r}, \quad (21)$$

and can be recast as $3/2 - \alpha$ for density profiles that can be approximated as power-law functions of radius over the radial width of the planet's horseshoe region. In Eq. (20), all terms are to be evaluated at the planet's orbital radius. This equation shows that in two-dimensional barotropic discs, the horseshoe drag cancels out when the surface density profile decreases locally as $r^{-3/2}$, while it is positive for density profiles shallower than $r^{-3/2}$. For density profiles strongly increasing outward, the horseshoe drag can be sufficiently positive to counteract the (negative) differential Lindblad torque, and therefore stall the migration of low-mass planets [71]. Such density jumps may be encountered near the star's magnetospheric cavity, or near the inner edge of a dead zone, across which the disc's effective turbulence decreases outward (the dead zone refers to the region near the midplane of protoplanetary discs that is sandwiched together by partially ionized surface layers).

The horseshoe drag expression in Eq. (20) exclusively holds in the case of barotropic discs. Those, naturally, are an idealised concept, and true discs have a more complex physics, which yields a more complex expression for the corotation torque. However, in any case, as we shall see, a common component of the corotation torque is given by Eq. (20), so that baroclinic effects yield additional terms to this expression.

We sum up the results presented in this section. In two-dimensional barotropic discs, where the gas pressure only depends on the surface density:

- The horseshoe drag is powered by the advection of the fluid's vortensity along horseshoe streamlines inside the planet's horseshoe region.
- It is proportional to the inverse vortensity gradient across the horseshoe region (that is, the quantity $3/2 + d \log \Sigma / d \log r$ for power law discs). It can therefore be negative, zero, or positive depending on the surface density gradient across the horseshoe region. For typical discs density and temperature profiles, its magnitude is smaller than that of the (negative) differential Lindblad torque.

3.2.4 Horseshoe drag in locally isothermal discs

A long considered framework, both in analytical and numerical studies is that of locally isothermal discs, in which the temperature is a fixed function of radius. No energy equation is considered in this case, but the flow is no longer barotropic: the pressure becomes a function of the density *and* position (through the temperature). The vortensity is no longer materially conserved. Its Lagrangian derivative features a source term arising from misaligned density and pressure gradients, or misaligned temperature and density gradients [58]:

$$\frac{D}{Dt} \left(\frac{\omega_z}{\Sigma} \right) = \frac{\nabla \Sigma \times \nabla P}{\Sigma^3} = \frac{\nabla \Sigma \times \nabla T}{\Sigma^2}. \quad (22)$$

As the temperature gradient has a radial direction and sensibly the same magnitude everywhere in the coorbital region, the strength of the source term depends on the density gradient: wherever the azimuthal density gradient is large, the source term is large. This occurs at the tip of the horseshoe U-turns where we have a strong azimuthal density gradient owing to the density enhancement in the planet's immediate vicinity. The time derivative in Eq. (22) can be expressed as a derivative with respect to the curvilinear abscissa s along the streamline:

$$\frac{D}{Ds} \left(\frac{\omega_z}{\Sigma} \right) = \frac{\nabla \Sigma \times \nabla T}{v \Sigma^2}, \quad (23)$$

where v is the norm of the fluid velocity in the corotating frame, where we have used $ds = v dt$. As the fluid stagnates in the vicinity of the stagnation point (*i.e.* v can be arbitrarily small, provided one chooses a streamline sufficiently close to the stagnation point), the source term of Eq. (23) formally diverges in the vicinity of the stagnation point. The total amount of vortensity created, integrated over the horseshoe streamlines, however, remains finite. Fig. 7 shows a vortensity map in the vicinity of a low-mass planet for a disc with $\alpha = 3/2$ (no background vortensity gradient) and $\beta = 1$ (uniform aspect ratio).

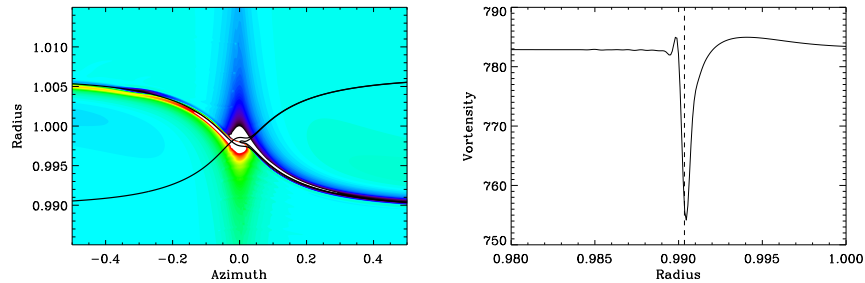


Fig. 7 Vortensity field in the coorbital region of a low-mass planet (left) and radial profile of vortensity at $\phi = +0.5$ rad (right), 30 orbital periods after the insertion of the planet. The disc has no background vortensity gradient, and a flat aspect ratio $H/r = 0.05$. Thin stripes of vortensity of opposite signs are clearly visible at the downstream separatrices. One can also see a mild production of vortensity in the wake, which fades away as one recedes from corotation, because of the winding of the wake and because fluid elements move faster away from corotation. Contrary to the adiabatic case that we shall present in § 3.2.5, the vortensity cut is not singular at the separatrix, as can be seen in the right panel. The radial resolution in the run presented is $9.3 \times 10^{-5} a$.

Thus far there is no rigorous mathematical proof that the horseshoe drag expression of Eq. (19) still holds in locally isothermal discs, as all demonstrations of that expression rely on the existence of a Bernoulli invariant, which does not exist in the locally isothermal case. Yet, data from numerical simulations suggest that this

expression is still valid in that regime. Assuming its validity from now on, we infer that the horseshoe drag must exhibit a dependence on the temperature gradient. The rationale for this being that the outgoing vortensity, accounted for by the horseshoe drag integral, includes the vortensity produced in the vicinity of the planet, which depends on the temperature gradient. Two-dimensional numerical simulations have confirmed the existence of an additional component of the corotation torque that depends on the temperature gradient [6, 14, 84]. The sign and value of this temperature-related corotation torque have a complex, and rather steep dependence with the softening length of the planet's potential [14]. Indeed, the topology of the horseshoe region depends heavily on the softening length: at large softening lengths, only one X-stagnation point is observed at corotation, in the planet vicinity, whereas at low softening lengths, two X-stagnation points are usually observed at corotation, on either side of the planet [14, 90]. The vortensity produced along a streamline depends on the path followed by the streamline. This situation is therefore much more complex than in the barotropic case or the adiabatic case that we present below, in which the existence of invariants under certain circumstances allows to get rid of the dependence on the actual path followed by fluid elements during their U-turns. Quite ironically, the locally isothermal case, which has served as a standard framework for more than two decades, is very difficult to tackle analytically.

The steep dependence of the temperature related corotation torque on the softening length appeals for a three-dimensional study of this torque, which is not plagued by softening issues. Such study has been undertaken by Casoli & Masset (in prep.), who find a linear dependence of the three-dimensional horseshoe drag on the temperature gradient $\beta = -d \log T / d \log r$, as steep as the dependence on the vortensity gradient \mathcal{V} given by Eq. (20).

3.2.5 Horseshoe drag in adiabatic discs

In the previous sections, the set of governing equations of the fluid did not include an energy equation, and the disc temperature, which was set as a prescribed function of radius, did not evolve in time. The first calculations undertaken with an energy equation were those of [77] and [86]. The former were devised in the shearing sheet framework, so that no net torque could be experienced by the planet, owing to the symmetry properties of the shearing sheet. Still, these authors found that radiative cooling could significantly affect the perturbed surface density pattern associated with the wakes, thus changing the magnitude of the one-sided Lindblad torque. [86] considered a planet in a three-dimensional disc, with an energy equation and thermal diffusion, and nested grids around the planet to achieve a very high resolution. They found that the migration of a low-mass planet could be reversed in sufficiently opaque discs, under the action of the corotation torque. The same result was in particular obtained in the adiabatic limit, which we are now going to focus on, as thermal diffusion yields an additional complexity, not needed at this stage. We will take thermal diffusion and other dissipative processes into account in § 3.3.

It was soon realised that the results of [86] were due to a new component of the corotation torque, linked to the entropy gradient [9, 88]. This is illustrated in Fig. 8, in which we compare the torque results for 69 different random disc profiles (the density slope α being a random variable uniformly distributed over the interval $[-3/2, +3/2]$, and the temperature slope β being an independent random variable uniformly distributed over the interval $[-2, +2]$.) Each calculation has a smoothing length of the planet's potential $\varepsilon = 0.3H$, and an aspect ratio at the planet location $h_p = 0.05$.

For each pair of α and β , we ran two calculations: a locally isothermal one, and an adiabatic one with a ratio of specific heats $\gamma = 1.4$. The torque difference, dubbed *adiabatic torque excess*, is then obtained by:

$$\Delta\Gamma_{\text{HS}}^{\text{entr}} = \Gamma_{\text{ad}} - \frac{\Gamma_{\text{iso}}}{\gamma}. \quad (24)$$

The correction of the isothermal torque Γ_{iso} by a factor γ^{-1} is necessary as both the differential Lindblad torque and the barotropic part of the horseshoe drag (the vortensity-related corotation torque) scale with the inverse square of the sound speed, which turns out in the adiabatic case to be $c_s^{\text{adi}} = c_s^{\text{iso}}\gamma^{1/2}$. The right part of Fig. 8 shows a clear one-to-one relationship between the adiabatic torque excess and the entropy gradient, irrespective of the individual values of α and β , which justifies the name *entropy-related corotation torque* given to the adiabatic torque excess. This torque is shown in two different regimes: the linear regime, soon after the insertion of the planet in the disc, and the horseshoe drag regime, reached after a longer timescale, as discussed in previous sections. As pointed out by [88], the non-linear corotation torque can be much larger (in this example, by a factor of about 5) than its linear counterpart, depending on the planet's softening length.

An interpretation of the entropy-related corotation torque was given soon after its discovery by [9] and [88]. Although this early interpretation was shown not to be quite correct when the horseshoe drag expression in the adiabatic case was worked out subsequently, we describe it here briefly as the mechanism on which it is based allows for a clear understanding of the correct origin of the entropy torque.

In an adiabatic disc, the entropy is materially conserved along the path of fluid elements, as long as they do not cross shocks, in a strict analogy with vortensity for barotropic flows. If we assume, for instance, a disc that has a positive radial entropy gradient prior to the planet insertion, outward horseshoe U-turns (behind the planet) bring to the outer side of the horseshoe region the low entropy of the inside. Similarly, inward horseshoe U-turns (ahead of the planet) bring to the inner side of the horseshoe region the high entropy of the outside. As the disc maintains a pressure equilibrium, the relative variations of the pressure across the coorbital region can be neglected, so that the surface density features relative variations opposite to that of the entropy, by virtue of the first order expansion of Eq. (1):

$$\gamma \frac{\delta\Sigma}{\Sigma} + \frac{\delta s}{s} = \frac{\delta P}{P} \approx 0. \quad (25)$$

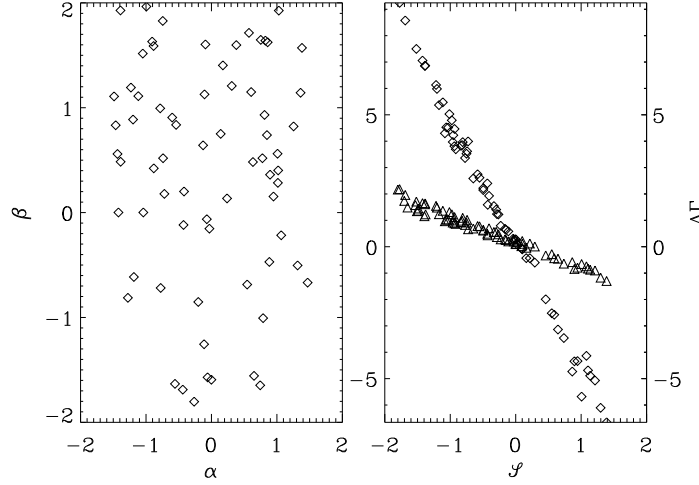


Fig. 8 Torque difference between the adiabatic and locally isothermal cases, given by Eq. (24), as a function of the entropy gradient (right panel), at early times (linear stage, triangles) and during the horseshoe drag stage (diamonds). The quantity \mathcal{S} in x-axis is defined in Eq. (30). Results have been obtained with calculations with random values of the surface density slope ($-\alpha$) and temperature slope ($-\beta$), shown in the left plot. The total number of runs is 138.

As a consequence, two lobes of perturbed surface density appear in the horseshoe region [9, 88, 44, 43], that both yield a torque of same sign. These two lobes are shown in Fig. 9.

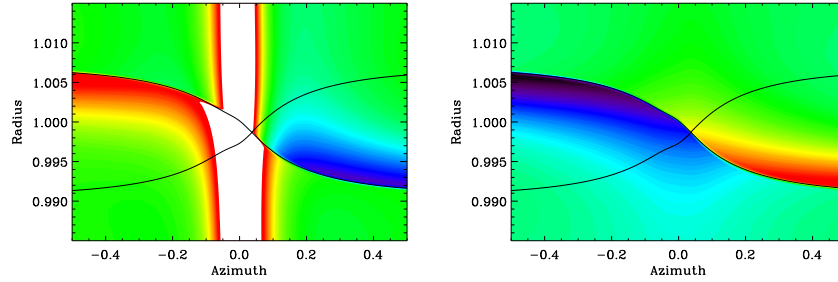


Fig. 9 Surface density perturbation in the planet's coorbital region of an adiabatic disc (left) and perturbation of entropy (right). The sign of the density lobes is opposite that of the entropy lobes. In addition to the lobes, the left plot also shows the wake, saturated in this representation. The background entropy profile increases with radius in this example.

The early interpretations identified the entropy related torque as the torque arising from the above density lobes. This explanation was appealing at first, because it gives the correct sign for the entropy related corotation torque, and the correct or-

der of magnitude: [9] performed an approximate, horseshoe-drag like integration to evaluate the impact of these lobes on the torque, whereas [88] performed an approximate direct summation. Both results were in rough agreement with the magnitude of the adiabatic torque excess, at least for the value of the potential softening length used in these studies. Yet, this explanation of the entropy torque quickly turned out not to be fully satisfactory, for the following reasons:

- Numerical explorations performed at different smoothing values showed that the entropy torque was approximately scaling as ε^{-1} , down to very low values of the smoothing length ($\varepsilon \sim 0.05H$). This apparent divergence of the entropy torque at low smoothing was incompatible with a scaling of the torque in x_s^4 , since the half-width x_s of the horseshoe region remains finite in the limit of a vanishing softening length [90].
- The saturation of the entropy torque was also problematic. We will examine saturation processes in detail in § 3.3, but for our purpose it suffices to know that the corotation torque always saturates in inviscid discs, that is to say tends to zero after a few libration timescales (as we have seen in Fig. 4). Therefore, one could devise a setup with an *inviscid* disc and finite thermal or entropy diffusion, which would forever maintain the same entropy perturbation within the horseshoe region (finite thermal diffusion is required in order to avoid phase mixing of entropy, as we shall see in § 3.3.2). As expected, the entropy related corotation torque is found to saturate as the disc is inviscid, while the (approximate) same density lobe structure is maintained within the horseshoe region [69]. This implies the density lobe structure would exert a torque at early times, but not at late times, which is contradictory.
- Finally, as we have seen in § 3.2.3, the density perturbation responsible for the corotation torque is not bound to the horseshoe region, but can extend further radially by the excitation of evanescent waves. In the barotropic case, the vortensity-related horseshoe drag is actually fully accounted for by an evanescent density distribution within the coorbital region. In the adiabatic case, attributing the entropy torque (*i.e.* the whole difference between an adiabatic and an isothermal calculation) to the density lobes was therefore tantamount to assuming that the evanescent wave structure in the coorbital region was the same in the adiabatic and isothermal cases, which is not obvious.

The identification of a convenient invariant of the flow for adiabatic discs with uniform temperature profile allowed [68, 69] to demonstrate that the horseshoe drag expression was exactly the same as that of the barotropic case, given by Eq. (19). In this case, the evaluation of the horseshoe drag amounts again to a budget of the vortensity entering or leaving the vicinity of the planet on horseshoe streamlines. An important consequence of this is that the torque due to the density lobes must not be incorporated manually, separately, into the corotation torque expression, and the whole problem of determining the horseshoe drag amounts to an evaluation of the vortensity distribution within the horseshoe region. Before we clarify this point, we stress that the vortensity distribution within the horseshoe region has the following features:

- Since the flow is baroclinic, vortensity is not materially conserved along streamlines. However, contrary to the locally isothermal case, the existence of a flow invariant in adiabatic discs with flat temperature profile allows an estimate of the vortensity acquired by a streamline during a U-turn, independently of its actual path [68].
- The vortensity created over the interior of the horseshoe region is very small, and has no impact on the torque, because it has same sign on both sides of the planet [68, 84].
- The main difference arises from a (formally) singular production of vortensity (or vorticity) on downstream separatrices, due to the entropy discontinuity at this location (which results from the entropy advection within the horseshoe region). This (formally) singular production of vortensity is readily apparent in the source term of Eq. (22), and is illustrated in Fig. 10. It can be evaluated analytically either using the flow invariant introduced in [68], or directly using Eq. (22) as in [84]. The first approach is self-contained and yields the amount of singular vortensity as a function of the flow properties at the stagnation point. The second is not restricted to flat temperature profiles, but it requires knowledge of the fluid velocity along horseshoe streamlines, which depends on the exact geometry of the horseshoe region, much like in locally isothermal discs discussed in § 3.2.4.

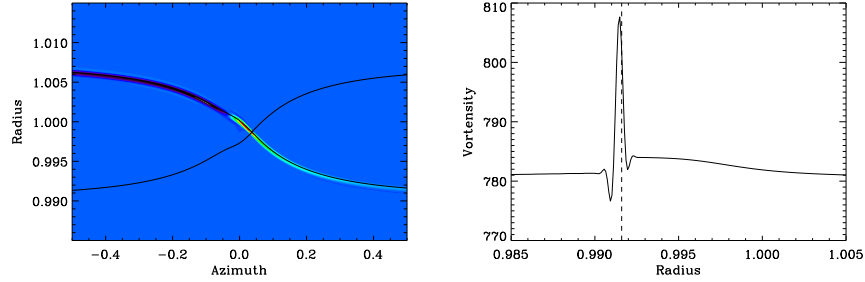


Fig. 10 Vortensity map in the coorbital region of an Earth-mass planet embedded in an adiabatic disc with $H = 0.05$ at the orbital radius of the planet (left), and radial profile of vortensity at $\phi = 0.5$ rad. (right), 60 orbital periods after the insertion of the planet in the disc. The grid resolution and disc gradients are the same as in Fig. 7 ($\alpha = 3/2$, $\beta = 0$). The vortensity peak has a much more compact profile than that of Fig. 7. This is to be expected as we have a singular vortensity sheet in the adiabatic case, and a continuous one, peaked at the separatrix, in the locally isothermal case.

We now clarify the contribution of the density lobes to the corotation torque. The corotation torque is directly related to the density perturbation within the corotation region, which can be written as

$$\frac{\delta\Sigma}{\Sigma} = \frac{1}{\gamma} \left(\frac{\delta P}{P} - \frac{\delta s}{s} \right), \quad (26)$$

where, counter to Eq. (25), we shall not assume $\delta P = 0$. The pressure perturbation δP can be shown to satisfy a second-order partial differential equation [68], with solution of the form:

$$\frac{\delta P}{P} = \gamma K * \frac{\delta u}{u}, \quad (27)$$

where $u = s^{1/\gamma} \times \Sigma / \omega_z$, $K \propto \exp(-|x|/H)$ is a Green kernel normalised to unity ($\int K(x) dx = 1$, with x the radial distance to the planet orbit), and H is the local pressure scale height. Further denoting the inverse vortensity by $l = \Sigma / \omega_z$, Eqs. (26) and (27) yield

$$\frac{\delta \Sigma}{\Sigma} = K * \left(\frac{\delta l}{l} + \frac{1}{\gamma} \frac{\delta s}{s} \right) - \frac{1}{\gamma} \frac{\delta s}{s}. \quad (28)$$

The first term on the right-hand side of Eq. (28) corresponds to the perturbed surface density associated to evanescent pressure waves (like in the barotropic case, where it reduces to $K * \delta l / l$), and the second term to the density lobes resulting from entropy advection. Since the convolution by the unitary function K in Eq. (28) does not change the linear mass of the perturbation ($\int \delta \Sigma(x) dx$), the corotation torque is the same as if, in the expression for the density perturbation in Eq. (28), the convolution product were actually discarded [68]. In the barotropic case for instance, this leads to the torque expression given by Eq. (19). In the adiabatic case, it shows that, counter-intuitively, the density lobes exert no *net* corotation torque. This further explains why, akin to the barotropic case, the calculation of the corotation torque comes to evaluating the vortensity distribution within the horse shoe region. Since the main difference in the vortensity field between the adiabatic and barotropic cases is the appearance of a singular sheet of vorticity at the downstream separatrices, and given that the magnitude of this sheet scales with the entropy gradient, this singular vorticity sheet can be unambiguously identified as the origin of the entropy-related torque.

Upon evaluation of the magnitude of the vorticity sheet at the separatrices, [68] inferred the following expression for the entropy-related corotation torque:

$$\Delta \Gamma_{\text{HS}}^{\text{entr}} = - \frac{1.3 \mathcal{S}}{\varepsilon / H} \Sigma \Omega_p^2 q^2 a^4 h^{-2}, \quad (29)$$

where the above expression has been derived in the framework of a flat temperature profile, and assuming a ratio of specific heats $\gamma = 1.4$. In Eq. (29), all disc quantities are to be evaluated at the planet's orbital radius, and the quantity \mathcal{S} is defined by

$$\mathcal{S} = \frac{1}{\gamma} \frac{d \log s}{d \log r}, \quad (30)$$

and can be recast as $[\beta + (\gamma - 1)\alpha] / \gamma$ for surface density and temperature profiles that can be approximated as power-law functions of radius over the planet's horse-shoe region.

Considering discs with arbitrary temperature profiles, [84] also evaluated the production of vortensity at downstream separatrices, which required estimating the ve-

locity along streamlines through a fit of numerical simulations. Unlike [68], they manually added the torque contribution from the density lobe structure. In the end, the latter remains small compared to the torque contribution from the singular sheet of vorticity. This explains why, overall, the derivations of the entropy-related corotation torque by [68] and [84] are in broad numerical agreement, within 30 %.

The generalisation to an arbitrary temperature profile of Eq. (29) cannot be tackled fully analytically, much as in the locally isothermal case. Yet, Eq. (24) shows that the adiabatic corotation torque is the sum of the entropy related term, given by Eq. (29), and the locally isothermal corotation torque (corrected by a factor γ). The latter is itself made up of two terms, as we have seen in sections 3.2.3 and 3.2.4. The corotation torque is therefore, in a general situation, the sum of three terms:

- The vortensity related torque, proportional to the vortensity gradient, and given by Eq. (20).
- The temperature related torque, proportional to the temperature gradient, discussed in section 3.2.4.
- The entropy related torque, proportional to the entropy gradient, given by Eq. (29).

It can be observed that there are only two degrees of freedom for the disc profiles (the density and temperature gradients α and β , or the vortensity and entropy gradients \mathcal{V} and \mathcal{S} , etc.), so that for a specific setup one may simplify the torque expression as a linear combination of the two independent parameters. This simplification is not desirable, however, because it blurs the distinct physical origin and characteristic of each of the three terms. Besides, one can disentangle these three terms by varying parameters such as the smoothing length ε or the ratio of specific heats γ . Any simplification of the torque expression is thus highly setup dependent.

Finally, we summarise the main message to take away about the corotation torque.

- In all cases it features a term that scales with the gradient of vortensity across the horseshoe region, given by Eq. (20). It has one or two additional terms, depending on whether an energy equation is taken into consideration. The first of those scales with the temperature gradient, and if an energy equation is included, there is a second one that scales with the entropy gradient.
- In all cases the corotation torque comes from the *vortensity* distribution in the horseshoe region. The additional contributions arise from the vortensity *created* by the temperature gradient and/or the entropy gradient.

3.3 Saturation properties of the horseshoe drag

We have described in Section 3.2 the physical origin and properties of the corotation torque in inviscid discs, with a special emphasis on the fully unsaturated horseshoe drag, which is the maximum value the corotation torque may take. This value is obtained about one horseshoe U-turn timescale after the planet insertion in the disc,

and is maintained over about half a libration timescale. Its sign and magnitude are determined by the gradients of vortensity, temperature and entropy across the horseshoe region.

In the absence of diffusion processes, after about half a libration timescale, the vortensity and entropy advected along the downstream separatrices of the horseshoe region reach the planet again, undergo another U-turn, and phase mixing starts to occur. Vortensity and entropy are progressively stirred up within the horseshoe region, and the horseshoe drag oscillates with time with a decreasing amplitude, as shown in Fig. 4. The horseshoe drag ultimately cancels out as both vortensity and entropy get uniformly distributed after several libration times [85, 69]. This is known as the horseshoe drag saturation.

Diffusion processes (viscosity, thermal diffusion) may maintain respectively the vortensity and entropy gradients across the horseshoe region, and thus sustain the horseshoe drag to a non-vanishing value. We review below the saturation properties of the horseshoe drag in barotropic discs (§ 3.3.1) and in radiative discs (§ 3.3.2).

3.3.1 Saturation properties of the vortensity-related horseshoe drag in barotropic viscous discs

In barotropic discs, the horseshoe drag saturates as vortensity is strictly advected along horseshoe streamlines. Viscosity acting as a diffusion source term in the vortensity equation can sustain a non-zero vortensity gradient across the horseshoe region. The vortensity-related horseshoe drag then attains a steady-state value, which arises from a net exchange of angular momentum between the horseshoe region and the rest of the disc [64, 65]. This steady-state value depends on how the viscous diffusion timescale across the horseshoe region (τ_{visc}) compares with the horseshoe libration timescale (τ_{lib}) and the horseshoe U-turn timescale ($\tau_{\text{U-turn}}$). Denoting by ν_p the kinematic viscosity at the planet location, $\tau_{\text{visc}} \sim x_s^2/\nu_p$. The libration timescale is given by Eq. (18), and the U-turn timescale is typically a fraction H/r of the libration timescale [9].

For the corotation torque to remain close to its maximum, fully unsaturated value in the long term, the inequality

$$\tau_{\text{U-turn}} \leq \tau_{\text{visc}} \leq \tau_{\text{lib}}/2, \quad (31)$$

should be verified. When the second inequality is satisfied, the vortensity at the upstream separatrices is kept stationary, which prevents phase mixing of vortensity within the horseshoe region [5, 64]. When the first inequality is satisfied, vortensity is approximately conserved along U-turns, which maximises the effective vortensity gradient across the horseshoe region [65, 69, 85]. Taking $x_s \sim 1.1a\sqrt{q/h_p}$ (as measured with a planet softening length $\approx 0.6H$), inequality (31) may be cast as

$$0.32q^{3/2}h_p^{-7/2} \leq \alpha_{\text{v,p}} \leq 0.16q^{3/2}h_p^{-9/2}, \quad (32)$$

where $\alpha_{v,p}$ and h_p denote the disc's alpha viscosity and aspect ratio at the planet location, respectively. The alpha viscosity for which the corotation torque takes its maximum value can be approximated as $0.16q^{3/2}h_p^{-4}$ [8].

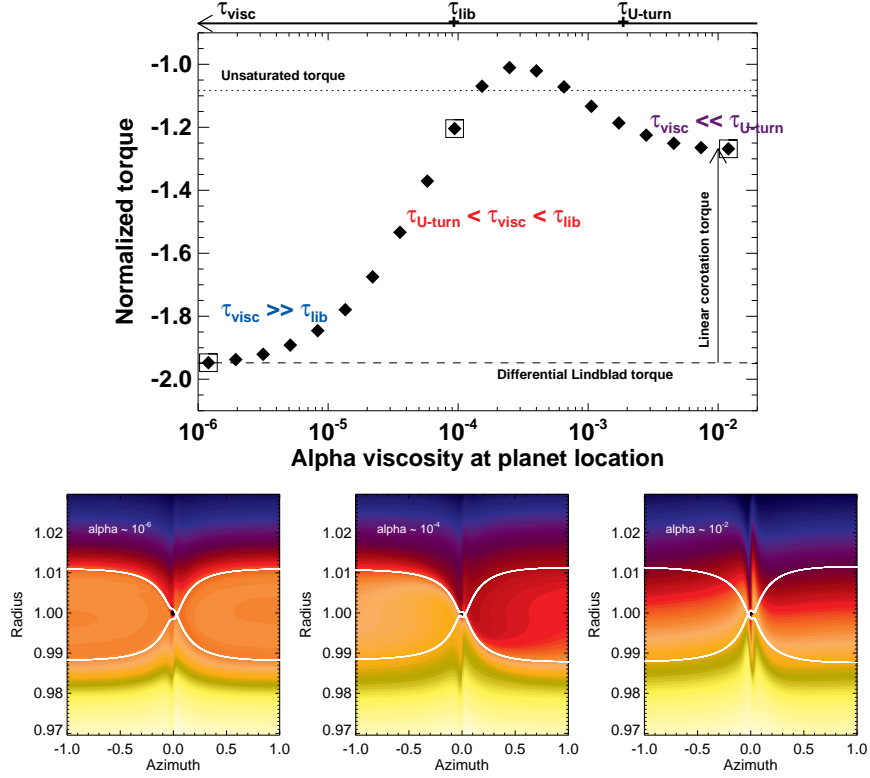


Fig. 11 Top: steady-state torque on a $M_p = 6 \times 10^{-6} M_*$ planet mass embedded in a thin ($h = 0.05$) disc for various alpha viscous parameters at the planet location. In this series of runs, $\alpha = 1/2$ and $\beta = 0$. Different saturation regimes of the corotation torque are illustrated, depending on how the viscous timescale across the planet's horseshoe region (τ_{visc}) compares with the horseshoe U-turn timescale ($\tau_{\text{U-turn}}$) and the libration timescale (τ_{lib}). The final torque value in an inviscid case, which reduces to the differential Lindblad torque, is shown by a dashed line. The fully unsaturated total torque (differential Lindblad torque plus fully unsaturated horseshoe drag) in an inviscid run is depicted by a dotted line. Bottom: vortensity distribution inside the planet's horseshoe region for the three alpha viscosities shown by squares in the top panel (viscosity increases from left to right). The separatrices of the horseshoe region are depicted by solid curves, and the planet position by a filled circle.

The saturation properties of the corotation torque are illustrated in Fig. 11 for a 2 Earth-mass planet embedded in a thin ($h_p = 0.05$) viscous disc. The background temperature profile is uniform, and the surface density decreases as $r^{-1/2}$. The top panel displays the steady-state torque at different alpha viscosities (a constant kin-

matic viscosity ν was used in the simulations). The left-hand term in inequality (32) is $\approx 1.7 \times 10^{-4}$, while the right-hand term is $\approx 1.7 \times 10^{-3}$, and it is clear from Fig. 11 that the corotation torque is maximum between these two alpha viscosities. When the viscosity is small enough so that $\tau_{\text{visc}} \gg \tau_{\text{lib}}$, viscosity is inefficient at restoring the vortensity gradient across the horseshoe region, and the horseshoe drag takes very small values (it saturates). At very large viscosities, such that $\tau_{\text{visc}} \ll \tau_{\text{U-turn}}$, the corotation torque plateaus at its value in the linear regime [89]. The vortensity distribution inside the horseshoe region for each saturation regime is shown in the bottom panels of Fig. 11. In the left panel, $\alpha_{\text{v,p}} \sim 10^{-6}$, and the steady-state vortensity distribution within the horseshoe region is uniform, resulting in a vanishing corotation torque. In the middle panel, $\alpha_{\text{v,p}} \sim 10^{-4}$ maintains a maximum vortensity contrast between the rear and front parts of the planet, with the consequence that the corotation torque is close to its fully unsaturated value. In the right panel, $\alpha_{\text{v,p}} \sim 10^{-2}$ imposes the initial (unperturbed) vortensity profile along the horseshoe U-turns, and the horseshoe drag therefore reduces to the linear corotation torque.

All attempts to capture analytically the saturation of the corotation torque have been carried out using a simplified streamline model that assumes the drift of the coorbital material with the velocity of the unperturbed disc, and which does not resolve spatially nor temporally the U-turns. This model was proposed in [64] and in a more formal manner in [69], where a numerical implementation of it is also described. All analytic works on the corotation torque saturation, whether they provide an asymptotic torque value [64, 69, 85] or they capture the time dependence of the torque in an inviscid disc [109] make use of this simplified model. Solving for the torque asymptotic value in this simplified advection-diffusion model can be tackled in a variety of ways. One such way consists of neglecting the azimuthal variation of the vortensity so as to reduce the advection-diffusion problem essentially to a one dimensional radial problem. This is the approach of [64] and [85]. These two works are quite different in their assumptions, and suffer from orthogonal restrictions:

- [64] exclusively contemplates the case of a disc with flat profiles of surface density and kinematic viscosity, so that his results must be rescaled by hand to apply to a general case. The approach used in this work considers the global angular momentum budget of the trapped horseshoe region, and relies upon the evaluation of the viscous friction of the disc on the separatrices. It also takes into account the viscous drift of material across the horseshoe region.
- [85] consider a disc with an arbitrary surface density gradient, and directly use the horseshoe drag integral of Eq. (19). Their model assumes no radial drift of disc material across the horseshoe region.

Quite remarkably, these two approaches yield the exact same result, which can be cast either in terms of Airy functions [64] or in terms of Bessel functions [85].

One can also solve the advection-diffusion equation satisfied by the fluid's vortensity in two dimensions, the solution being exact in the limit of a small viscosity. In this limit, the problem amounts to an alternation of convolutions (viscous diffusion of vortensity between two successive horseshoe U-turns) and reflections

(mapping of vortensity – or, vortensity conservation – from one tip of the horseshoe region to the other during a U-turn). This is the approach of [69], who also discards the possible radial drift of disc material across the horseshoe region. The dependence thus obtained — equation (119) of [69] — is broadly the same as that of [64] and [85], but reproduces more closely the results from numerical simulations. We note that the decay of the torque value found at large viscosity (see Fig. 11), which corresponds to a decay towards the linear corotation torque value [89], has not yet been described analytically in a self-contained manner. [69] and [85] use an ad-hoc reduction factor, either with one free parameter [69] or two free parameters [85], the value of the free parameters being inferred from numerical simulations.

In summary, in barotropic discs, vortensity essentially obeys an advection-diffusion equation in the coorbital region. When the viscous diffusion timescale across the horseshoe region is:

- Long compared to the libration period, vortensity is progressively stirred up and the corotation torque ultimately saturates (tends to zero).
- Short compared to the libration period, but long compared to the horseshoe U-turn time, the corotation torque is close to its fully unsaturated, maximum value.
- Short compared to the horseshoe U-turn time, the corotation torque tends to its value predicted in the linear regime.

3.3.2 Saturation properties of the horseshoe drag in radiative discs

Much as in barotropic discs, the estimate of the asymptotic corotation torque value in radiative discs amounts to the determination of the vortensity distribution within the horseshoe region at later times. There is an additional complexity, however, due to the fact that this is no longer an advection-diffusion problem, but an advection-diffusion-creation problem, as vortensity is created during the U-turns (see section 3.2.5, and in particular Fig. 10). Furthermore, the amount of vortensity created depends on the entropy distribution, as was explained in section 3.2.5. This analysis was undertaken by [85] in the case of a unitary thermal Prandtl number (the viscosity ν and thermal diffusion χ have same value). A corotation torque expression was proposed by these authors, as a result of a fit of numerical simulations. Under the assumption of a unitary Prandtl number, the parameter space to be explored is one-dimensional, and for a (common) value of ν and χ , the radiative torque is found to saturate more easily than the barotropic torque. This is interpreted by the authors as due to the fact the entropy-related corotation torque is essentially due to a unique streamline, where the advection speed is maximal (that of the separatrices).

To relax the assumption of a unitary Prandtl number, one may assume that the torque dependence upon viscosity or thermal diffusion have the same shape, which allows to propose a formula with two independent parameters ν and χ , which can then be validated by checking its accuracy with numerical simulations. This is the approach adopted by [85]. Another solution consists in using a streamline model such as the one outlined in section 3.3.1. This is the approach of [69]. As the vortensity is now determined by an advection-diffusion-creation problem, one needs to

amend the barotropic model of section 3.3.1 by adding the creation of vortensity during the U-turns, which is determined by the entropy field. Therefore, prior to the determination of the vortensity distribution, an analysis of the entropy distribution at later times is required. This preliminary determination can be done easily, because the entropy obeys an advection-diffusion problem formally equivalent to the vortensity distribution in the barotropic case, in which one replaces the vortensity with the entropy, and the viscosity ν with the thermal diffusion χ . Once the entropy distribution within the horseshoe region is known, the vortensity distribution at late times is obtained, which allows, upon the use of the horseshoe drag expression of Eq. (19), for an expression of the corotation torque as a function of viscosity and thermal diffusivity, and which can be checked *a posteriori* against numerical simulations.

The corotation torque expressions, as a function of viscosity and thermal diffusivity, are given by Eqs. (161-164) of [69], or by Eqs. (52-53) of [85].

3.4 Type I migration in turbulent discs

We have examined in the previous sections the properties of planet-disc interactions assuming viscous discs, described with a stationary kinematic viscosity aimed at modelling their turbulent transport properties. Because the corotation torque may play a dramatic role in the orbital evolution of low-mass planets, and its magnitude is intimately related to diffusion processes taking place within the planet's horseshoe region, it is relevant to determine how turbulence may impact type I migration.

Turbulence in protoplanetary discs can have a variety of origins. These include hydrodynamic instabilities, such as Rossby-wave instabilities [58], the global baroclinic instability [42, 59], the sub-critical baroclinic instability [49], planetary gap instabilities [55, 56] (which we will discuss in § 4.2), or the Kelvin-Helmholtz instability triggered by the vertical shear of the gas as dust settles into the mid plane [41]. Convective instability might also be relevant in the inner parts of massive discs, and it would be interesting to examine its impact on type I migration. Perhaps the most likely source of turbulence in protoplanetary discs is the magnetohydrodynamic (MHD) turbulence resulting from the magnetorotational instability (MRI) [4]. It relies on the coupling of the ionised gas to the weak magnetic field in the disc. Ionisation may occur in the vicinity of the central object due to the star's irradiation, or further out in the disc layers, most probably through the UV background or cosmic rays. It is currently debated which regions of planet formation near the disc mid plane are sufficiently ionised ('active') to trigger the MRI, and which ones remain neutral (which is usually referred to a 'dead zone'). In the latter case, some transport of angular momentum would still be present through the propagation of waves induced by MHD turbulence in the disc's upper layers [27]. The alpha viscous parameter associated to MHD turbulence is typically in the range $[5 \times 10^{-3} - 5 \times 10^{-2}]$ in active regions, while being about two orders of magnitude smaller in dead zones.

The properties of type I migration in weakly magnetised turbulent discs have been investigated in a couple of studies. [82] performed 3D simulations of locally

isothermal discs fully invaded by MHD turbulence. They found that the running time-averaged torque on a fixed protoplanet experiences rather large-amplitude oscillations over the reduced temporal range over which the simulation could be run, and that its final value differs quite substantially from the torque value expected in viscous disc models. Similar results were obtained by [80], who allowed the planet orbit to evolve. A primary reason for the observed difference between the viscous torque and the time-averaged turbulent torque is that the 3D MHD simulations were not converged in time. This was suggested by [8], who considered 2D isothermal discs subject to stochastic forcing, using the turbulence model originally developed by [48]. They showed indeed that when time-averaged over a sufficiently long time period, which may be as long as a thousand orbits, both the differential Lindblad torque and the corotation torque behave very similarly as in equivalent viscous disc models. These results were essentially confirmed by the 3D MHD simulations by [7], who adopted a locally isothermal disc model with a mean toroidal magnetic field, in which non-ideal MHD effects and vertical stratification were neglected (see illustration in Fig. 12). Similar agreement was obtained by [104] with vertical stratification. Nonetheless, [7] found an additional corotation torque with moderate magnitude in their 3D MHD simulations, related to the presence of a mean toroidal magnetic field. The existence and properties of this additional corotation torque have been explored by Guilet, Baruteau & Papaloizou (in prep.) in 2D weakly magnetised, non-turbulent disc models, in which the effects of turbulence are modelled by viscous and magnetic diffusivities. They find that the additional corotation torque can take large values, and even exceed the differential Lindblad torque, depending on the disc's viscous and magnetic diffusivities, and the amplitude of the background magnetic field.

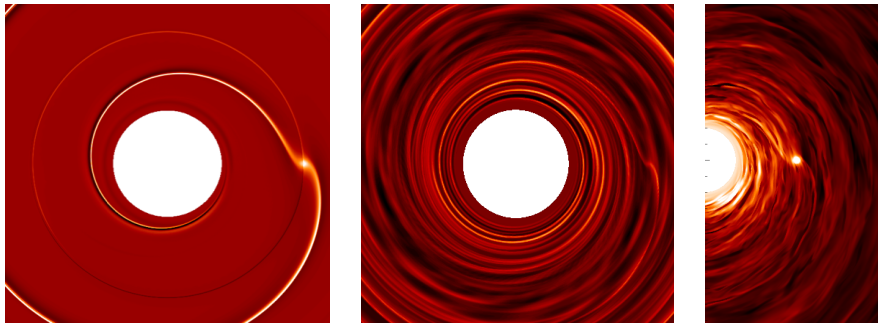


Fig. 12 Perturbation of the disc's density by an embedded planet. Left: adiabatic two-dimensional disc. The density lobes within the coorbital region, which arise from the advection of entropy, help identify the (tiny) radial width of the planet's horseshoe region. Middle: case of an isothermal 2D disc with turbulence induced by stochastic stirring. Right: case of an isothermal 3D disc invaded by MHD turbulence due to the MRI (the density in the disc mid plane is displayed). In the middle and right panels, the turbulent density perturbation is comparable to the perturbed density associated to the planet's wakes. Images taken from [6, 8, 7], respectively.

The aforementioned results were for embedded planets with a horseshoe radial width that is a moderate fraction of the disc’s pressure scaleheight, the latter being the typical size of turbulent eddies. The existence of horseshoe dynamics and a corotation torque is unknown for planets with a horseshoe region width that is a small fraction of the turbulent eddy size. In this case, it is possible that turbulence acts more as a source of random advection of vortensity through the horseshoe region, rather than diffusion.

4 Migration of gap-opening planets: Type II and III migration

The disc response to a low-mass planet has been studied in details in § 3, where we have focused on the two components of the type I migration torque. The aim of this section is to examine the range of planet masses that is relevant to type I migration in § 4.1, and to give a concise description of planet–disc interactions for planets that are massive enough to significantly perturb the disc’s mass distribution (§ 4.2 and 4.3).

4.1 Shock formation and gap-opening criterion

The wakes generated by a planet in a disc carry angular momentum as they propagate away from the planet. This angular momentum is eventually deposited in the disc through some wave damping processes, which leads to redistributing the disc mass. An efficient wave damping mechanism relies on the non-linear wave evolution of the wakes into shocks [33]. The (negative) angular momentum deposited by the inner wake decreases the semi-major axis of the fluid elements in the disc region inside the planet’s orbit (the inner disc). Similarly, the (positive) angular momentum deposited by the outer wake increases the semi-major axis of the fluid elements in the outer disc.

The distance d_s from the planet where the planet-generated wakes become shocks is given by [33, 25]:

$$d_s \approx 0.8 \left(\frac{\gamma+1}{12/5} \frac{q}{h^3} \right)^{-2/5} H(a), \quad (33)$$

where γ is the gas adiabatic index, and a denotes the planet’s semi-major axis. As the magnitude of the one-sided Lindblad torque peaks at $\sim 4H(a)/3$ from the planet’s orbit, a linear description of the differential Lindblad torque thus fails when $|d_s| \sim 4H(a)/3$. This condition can be recast as $q \sim 0.3h^3$ for $\gamma = 5/3$. When $|d_s| \leq 2H(a)/3$, wakes turn into shocks within their excitation region. Fluid elements just outside the planet’s horseshoe region are pushed away from the planet orbit after crossing the wakes, which directly affects the planet’s coorbital region by inducing asymmetric U-turns [66]. Horseshoe fluid elements therefore get pro-

gressively repelled from the planet orbit after each U-turn, and the planet slowly depletes its coorbital region. The equilibrium structure (width, depth) of the annular gap the planet forms around its orbit is determined by a balance between gravity, viscous and pressure torques [18].

Shock formation and its damping efficiency are very sensitive to the disc's viscosity, and gap-opening results from a balance between (i) a planet mass large enough to induce shocks where the wake excitation takes place, and (ii) a viscosity small enough to maximise the amount of angular momentum deposited by the shocks in the planet's immediate vicinity:

1. The first condition reads $|d_s| \leq 2H(a)/3$, which corresponds to $q \geq 1.5h^3$ for $\gamma = 5/3$. It means that the planet's Bondi radius $r_B = GM_p/c_s^2$, where the pressure distribution is most strongly perturbed by the planet, as well the planet's Hill radius become comparable to the local pressure scaleheight. This is known as the thermal criterion for gap opening [53].
2. The second condition, known as the viscous criterion, can be expressed as $q \geq 40/\mathcal{R}$, where $\mathcal{R} = a_p^2 \Omega_p / \nu$ is the Reynolds number¹ [51, 13].

The above two conditions for gap-opening have been revisited by [18], who provide a unified criterion that takes the form

$$1.1 \left(\frac{q}{h^3} \right)^{-1/3} + \frac{50\alpha_v h^2}{q} \leq 1, \quad (34)$$

where we have written the disc's kinematic viscosity $\nu = \alpha_v h^2 a^2 \Omega$ [100], and where in Eq. (34) h and α_v are to be evaluated at the planet's semi-major axis. An illustration of the smallest planet mass opening a gap according to criterion (34) is shown in Fig. 13, where it is clear that the gap-opening mass increases with increasing disc viscosity and aspect ratio. Assuming $h \approx 0.05$, which may be typical of planet forming regions, the gap-opening mass is in the Saturn-mass range for regions with low turbulent activity (dead zones, with typically $\alpha_v \sim 10^{-4}$), and is in the Jupiter-mass range in regions where $\alpha_v \sim 10^{-2}$. Note that when disc self-gravity is included, the gap-opening criterion of Eq. (34) should involve the effective planet mass, that is the sum of the planet and circumplanetary disc masses, rather than the planet mass alone.

Prior to a depletion of their coorbital region due to shock formation at the wake's excitation region, planets with increasing mass experience a flow transition in their immediate vicinity. The flow passes from a low-mass planet configuration described in section 3.2.1 and Fig. 3, to a high-mass configuration, where fluid elements may become trapped inside a circumplanetary disc around the planet. This flow transition is accompanied by a rapid increase in the half-width x_s of the horseshoe region, from a fluid-dominated regime (where $x_s \propto (q/h)^{1/2}$) to a gravity-dominated regime

¹ Although traditionally dubbed Reynolds number essentially for dimensional considerations, this ratio has little to do with the dimensionless ratio that must be considered to assess whether a flow is laminar or turbulent. If one regards the planet as an obstacle in the sheared Keplerian flow, it would be more appropriate to consider as a characteristic scale the size of its Roche lobe or $\sim x_s$, and as a characteristic velocity $2|A|x_s$.

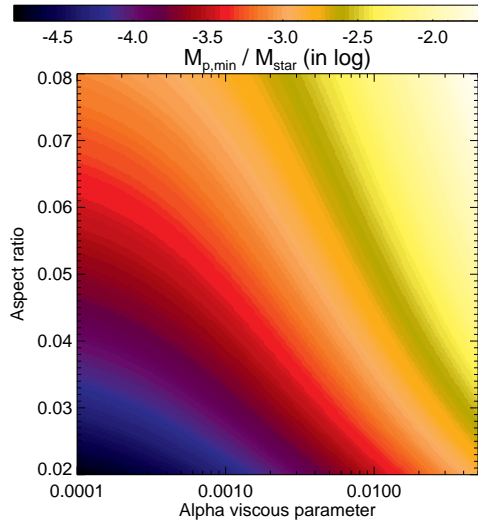


Fig. 13 Minimum planet-to-primary mass ratio leading to gap-opening as a function of the disc’s alpha viscous parameter (x-axis) and aspect ratio (y-axis) at the planet’s semi-major axis. This minimum mass is calculated numerically using criterion (34).

(where $x_s \sim R_H \propto q^{1/3}$) [70]. This rapid increase yields a significant increase in the corotation torque, as the latter scales as x_s^4 . This effect is found to be most significant for planet-to-primary mass ratios $q \sim 0.6h^3$ [70], which corresponds to 20 Earth-mass planets in $h = 0.05$ discs. It may contribute to further slowing down, or even reversing the migration of growing planets before they carve a gap around their orbit [23, 70].

4.2 Partial gap-opening: type III migration in massive discs

So far, we have addressed the properties of planet migration through a direct analysis of the tidal torque, the latter being directly proportional to the migration rate, see Eq. (7). This approach is valid for low-mass planets that do not open a gap, for which migration has a negligible feedback on the tidal torque (note that a weak, negative feedback slightly decreases the magnitude of the entropy-related horseshoe drag [68]). Nevertheless, migrating planets that open a partial gap around their orbit experience an additional corotation torque due to fluid elements flowing across the horseshoe region [72]. If for instance the planet migrates inwards, fluid elements circulating near the inner separatrix of the horseshoe region enter the horseshoe region, and execute an outward U-turn when they reach the vicinity of the planet. Upon completion of the U-turn, these fluid elements leave the horseshoe region as the planet keeps migrating, and end up circulating in the outer disc. Consequently, the mass distribution within the horseshoe region may become asymmetric, as the horseshoe region adopts approximately a trapezoidal shape in the azimuth-radius plane [72]. As a consequence, in the case of an inward migrating planet, there is

more mass behind the planet than ahead of it, owing to the partial depletion of the asymmetric horseshoe region. This point is illustrated in the left panel of Fig. 14. Similarly, if the planet migrates outwards, fluid elements circulating near the outer separatrix may embark on single inward U-turns across the horseshoe region.

Assuming steady migration at a moderate rate (this point will be clarified below), the additional corotation torque experienced by the planet due to the orbit-crossing flow is, to lowest order in x_s/a ,

$$\Gamma_{\text{cross}} = 2\pi a \dot{a} \Sigma_s \times 4Bax_s, \quad (35)$$

where Σ_s is the surface density at the inner (outer) horseshoe separatrix for a planet migrating inwards (outwards). The term $2\pi a \dot{a} \Sigma_s$ in the right-hand side of Eq. (35) is the mass flux across the horseshoe region. The second term ($4Bax_s$) is the amount of specific angular momentum that a fluid element near a horseshoe separatrix exchanges with the planet when performing a horseshoe U-turn. Note that the above expression for Γ_{cross} assumes that all circulating fluid elements entering the coorbital region embark on horseshoe U-turns, whereas a fraction of them may actually become trapped inside the planet's circumplanetary disc. Since Γ_{cross} is proportional to, and has same sign as \dot{a} , migration may become a runaway process. We now discuss under which circumstances a runaway may happen.

The planet and its coorbital material (which encompasses the horseshoe region, with mass M_{hs} , and the circumplanetary disc, with mass M_{cpd}) migrate at the same drift rate, \dot{a} , which we assume to be constant. The rate of angular momentum change of the planet and its coorbital region includes (i) the above contribution Γ_{cross} to the corotation torque, and (ii) the tidal torque that, for planets opening a partial gap, essentially reduces to the differential Lindblad torque Γ_{LR} :

$$2Ba\dot{a}(M_p + M_{\text{cpd}} + M_{\text{hs}}) = 2\pi a \dot{a} \Sigma_s \times 4Bax_s + \Gamma_{\text{LR}}. \quad (36)$$

Eq. (36) can be written as

$$2Ba\dot{a}\tilde{M}_p = 2Ba\dot{a}\delta m + \Gamma_{\text{LR}}, \quad (37)$$

where $\tilde{M}_p = M_p + M_{\text{cpd}}$ corresponds to an *effective* planet mass, and where $\delta m = 4\pi a x_s \Sigma_s - M_{\text{hs}}$ is called the coorbital mass deficit [72]. It represents the difference between (i) the mass the horseshoe region would have if it had a uniform surface density equal to that of the separatrix-crossing flow, and (ii) the actual horseshoe region mass.

The migration rate of a partial gap-opening planet, given by Eq. (37), can be described as a feedback loop [66]. This is illustrated in the right panel of Fig. 14, where the loop input is the differential Lindblad torque, and its output is the migration rate. When $\delta m < \tilde{M}_p$, the feedback loop remains stable. The drift rate in this case is not strictly a type I nor a type II migration rate. It is rather a type I rate enhanced by coorbital effects. No special name has been assigned to this kind of migrating regime. When $\delta m > \tilde{M}_p$, the feedback loop gets unstable, and migration enters a runaway regime, which can be either inward or outward. The drift rate as

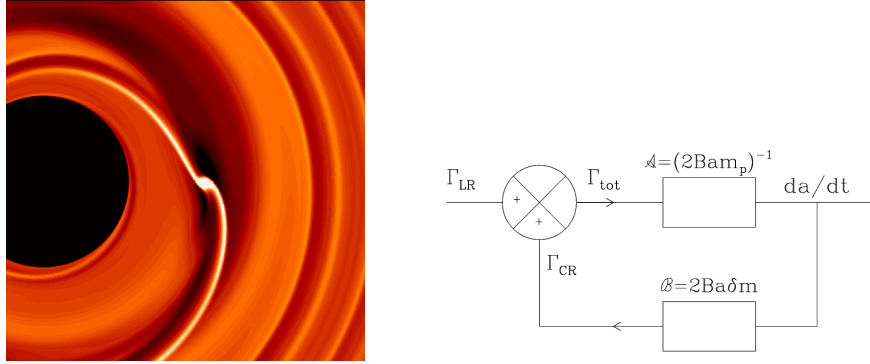


Fig. 14 Left: illustration of the flow asymmetry ahead of and behind a Saturn-mass planet undergoing rapid inward runaway migration. Right: type III planetary migration seen as a feedback loop. The latter remains stable if the open-loop transfer function $\mathcal{A} \times \mathcal{B} < 1$, or $\delta m < M_p$. From [66].

a function of the disc mass undergoes a bifurcation [66], and this regime is called runaway type III migration [72, 94, 95].

Runaway migration is based on the planet's ability to build up a coorbital mass deficit by opening a gap. It does not apply to low-mass planets, for which $\delta m \ll \tilde{M}_p$. It does not apply to high-mass planets neither, which open a wide, deep gap, so that the surface density of the separatrix-crossing flow is too small to produce a significant mass deficit. It rather concerns intermediate-mass planets, marginally satisfying the gap-opening criterion in Eq. (34), in massive discs (the larger the disc mass, the larger the density of the orbit-crossing flow). Its occurrence is illustrated in Fig. 15 for a disc with aspect ratio $h = 5\%$ and alpha viscosity $\alpha_v = 4 \times 10^{-3}$, where we see that runaway migration may be particularly relevant to Saturn-mass planets in massive discs (with a Toomre-Q parameter at the planet's orbital radius typically less than about 10). Bear in mind, however, that the occurrence for runaway migration is sensitive to the values of h and α_v , since they affect the planet's ability to open a partial gap. Also, note that the criterion for runaway migration features the *effective* planet mass \tilde{M}_p , sum of the planet mass and the circumplanetary disc mass. The occurrence for runaway migration is therefore sensitive to the mass distribution inside the circumplanetary disc, which may be significantly affected by the assumed physical modelling, e.g., whether gas accretion on the planet is taken into account [24], the inclusion of self-gravity [112], or the treatment for the gas thermodynamics [93]. It may also be affected by grid resolution effects in numerical simulations [20, 93].

The simple model described above helps understand the condition for migration to enter a runaway regime. However, since it assumes steady migration (that is, constant \dot{a}), this model is no longer valid when migration actually enters the runaway regime, where the migration rate increases exponentially over a time comparable to the horseshoe libration period. A more general approach can be found in [72, 66, 94]. As long as the orbital separation by which the planet migrates over a libration period remains smaller than the radial width of the planet's horseshoe

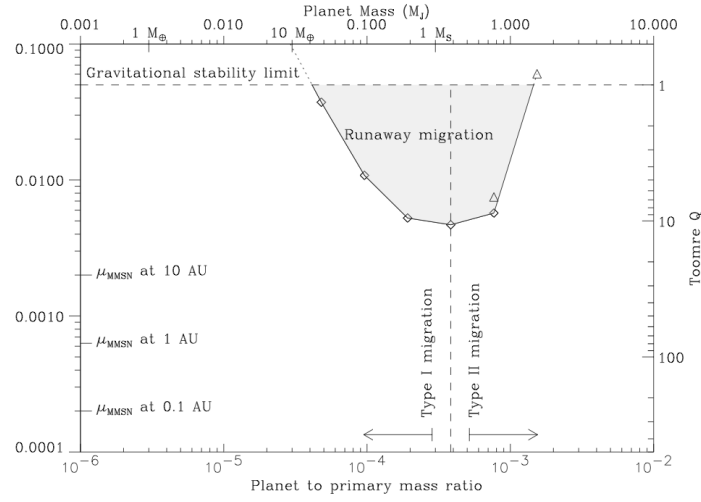


Fig. 15 Occurrence for type I, II and III (runaway) migrations with varying the planet-to-primary mass ratio (bottom x -axis) and the disc-to-primary mass ratio (left y -axis). The disc's aspect ratio is $h = 0.05$ and its alpha viscosity is $\alpha_v = 4 \times 10^{-3}$. The right y -axis shows the Toomre Q -parameter at the planet location. The upper part of the plot is limited by the gravitational instability limit (dashed line). From [72].

region, Γ_{cross} remains approximately proportional to \dot{a} (slow runaway regime). At larger migration rates (fast runaway regime), Γ_{cross} reaches a maximum and slowly decreases with increasing \dot{a} [72] (see also Fig. 16 in [66]). The precise dependence of Γ_{cross} with \dot{a} in this fast runaway regime is intrinsically related to the evolution of the mass coorbital deficit, and therefore to the planet's migration history. The orbital evolution of planets subject to runaway type III migration is therefore difficult to predict. Numerical simulations find that, depending on the resolution of the gas flow surrounding the planet, the timescale for inward runaway type III migration can be as short as a few 10^2 orbits [72, 15].

The sign of Γ_{cross} is dictated by the initial drift of the planet. Runaway migration can therefore be directed inwards or outwards, depending on the sign of \dot{a} before the runaway takes place. In particular, migration may be directed outwards if, despite the coorbital region being partly depleted, a (positive) horseshoe drag remains strong enough to counteract the (negative) differential Lindblad torque. Outward runaway migration could thus be an attractive mechanism to account for the recent discovery of massive planets at large orbital separations (which we will further discuss in § 5.1). Simulations [72, 66, 95] however show that, despite the expected increase in the mass of the orbit-crossing flow as the planet moves outwards (for background surface density profiles shallower than r^{-2}), the mass coorbital deficit cannot be retained indefinitely. The increase in the mass of the circumplanetary disc, and the strong distortion of the flow within it at large migration rates, lead the planet to

eventually lose its coorbital mass deficit, and the sense of migration is found to reverse.

Type III migration has been recently revisited in low-viscosity discs ($\alpha_v \leq$ a few $\times 10^{-4}$). Depending on the disc mass, the edges of the planet-induced gap may be subject to two kinds of instabilities. In low-mass discs, gap edges are unstable to vortex-forming modes [58, 50, 56]. They lead to the formation of several vortices sliding along the gap edges, which merge and form large-scale vortices. When they pass by the planet, these vortices may embark on horseshoe U-turns and exert a large corotation torque on the planet, with the consequence that the planet can be scattered inwards or outwards [54]. When the fluid’s self-gravity is taken into account, only a fraction of the large-scale vortices actually embark on horseshoe U-turns, the rest of the vortices keeps on sliding along the gap edges. This provides a periodic, intermittent corotation torque on the planet. Depending on the relative strengths of the vortices embarking on inward and outward U-turns, this mechanism acts much like an intermittent type III migration regime. In massive self-gravitating discs (stable against the gravitational instability), vortex-forming modes are replaced by global edge modes, which excite spiral density waves [55]. A decreasing radial profile of the Toomre-Q parameter favours edge modes at the gap’s outer edge. The periodic protrusion of edge mode-induced density waves near the gap’s outer edge provides a periodic source of (positive) corotation torque on the planet, and induces an intermittent type III migration regime. Numerical simulations by [57] show that edge modes can sustain outward migration, until the planet leaves its gap.

We briefly sum up the main results of this paragraph:

- Migrating planets experience an additional corotation torque due to fluid elements flowing across the horseshoe region, and embarking on horseshoe U-turns. It is proportional to the planet’s migration rate at small migration rates, which gives a positive feed back on migration. When the feedback loop diverges, the migration type is known as type III migration.
- The planet and its circumplanetary disc feel an effective corotation torque that is proportional to the coorbital mass deficit, defined through Eq. (37). The occurrence of a runaway feedback (*i.e.* of type III migration) corresponds to the coorbital mass deficit exceeding the mass of the planet and its circumplanetary disc. This applies to planets opening a partial gap around their orbit in massive protoplanetary discs.
- The orbital evolution of planets undergoing type III migration is sensitive to the time evolution of the coorbital mass deficit, which makes it difficult to predict. Numerical simulations show that runaway migration operates on very short timescales, typically in 100 to 1000 planet orbits.

4.3 Deep gap-opening: Type II migration

Planets massive enough to clear their coorbital region and open a deep gap around their orbit (see illustration in Fig. 16) enter the migration regime called Type II

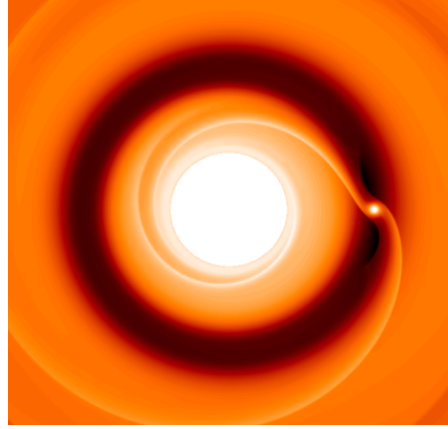


Fig. 16 Gap opened by a Jupiter-mass planet orbiting a Sun-like star.

migration. Such planets satisfy the gap-opening criterion given by Eq. (34). Assuming, for instance, a protoplanetary disc with aspect ratio $\sim 5\%$ and alpha viscosity $\alpha_v \sim 10^{-2}$, type II migration typically applies to planets more massive than Jupiter orbiting Sun-like stars. Compared to the type I and type III migration regimes described previously, the amplitude of the corotation torque is much reduced due to the clearing of the planet's coorbital region, and the differential Lindblad torque balances the viscous torque exerted by the disc. The net torque on the planet can be written as a fraction C_{II} of the viscous torque due to the outer disc [17]. This factor C_{II} features the time-dependent fraction of gas f_{gas} remaining in the planet's coorbital region.

The particular case with f_{gas} going to zero corresponds to what is usually referred to as standard type II migration regime. Its timescale can be approximated as

$$\tau_{\text{II}} \approx \frac{2r_o^2}{3\nu(r_o)} \left(1 + \frac{M_p}{4\pi\Sigma(r_o)r_o^2} \right), \quad (38)$$

where ν denotes the disc's kinematic viscosity, Σ the surface density of the disc perturbed by the planet, and r_o is the location in the outer disc where most of the planet's angular momentum is deposited. It can be approximated as the location of the outer separatrix of the planet's horseshoe region, which, for gap-opening planets, is $r_o \approx a + 2.5R_{\text{H}}$ [70]. The first term on the right-hand side of Eq. (38) corresponds to the viscous drift timescale at radius r_o , and the second term features the ratio of the planet mass to the local disc mass at radius r_o . Two migration regimes can therefore be distinguished:

1. *Disc-dominated type II migration.* When the planet mass is much smaller than the local disc mass (by which we refer to the quantity $4\pi\Sigma(r_o)r_o^2$), the planet behaves much like a fluid element that the disc causes to drift viscously. The planet's migration timescale then matches the disc's viscous drift timescale $\approx 2r_o^2/3\nu(r_o)$ [52]. In this migration regime, called disc-dominated type II migration, the planet remains confined within its gap. Should the planet migrate slightly faster than

the disc near its orbit, the increased inner Lindblad torque due to the planet getting closer to the gap's inner edge would push the planet outward. Conversely, should the planet migrate at a slower pace than the (local) disc, the increased outer Lindblad torque would push the planet back inward. The timescale for the disc-dominated type II migration regime, $\tau_{\text{II,d}}$, can be recast as

$$\tau_{\text{II,d}} \approx 4.7 \times 10^4 \text{ yrs} \times \left(\frac{\alpha_v}{10^{-2}} \right)^{-1} \left(\frac{h}{0.05} \right)^{-2} \left(\frac{M_\star}{M_\odot} \right)^{-1/2} \left(\frac{r_o}{5 \text{ AU}} \right)^{3/2}, \quad (39)$$

where α_v and h are to be evaluated at r_o .

2. *Planet-dominated type II migration.* When the planet mass becomes comparable to, or exceeds the local disc mass, the orbital evolution of a gap-opening planet is no longer dictated by the disc alone. The inertia of the planet slows down its orbital migration [101, 39], and in the limit when the planet mass is large compared to the local disc mass, the planet enters the so-called planet-dominated type II migration regime, whose timescale $\tau_{\text{II,p}}$ reads

$$\tau_{\text{II,p}} \approx \tau_{\text{II,d}} \times \left(\frac{M_p}{4\pi\Sigma(r_o)r_o^2} \right), \quad (40)$$

with $\tau_{\text{II,d}}$ given by Eq. (39), and where the planet to local disc mass ratio reads

$$\frac{M_p}{4\pi\Sigma(r_o)r_o^2} \approx 200 \left(\frac{M_p}{M_\odot} \right) \left(\frac{\Sigma(r_o)}{150 \text{ g cm}^{-2}} \right)^{-1} \left(\frac{r_o}{5 \text{ AU}} \right)^{-2}. \quad (41)$$

In self-gravitating discs, the distinction between the planet- and disc-dominated type II migration regimes should involve the comparison between the local disc mass and the effective planet mass \tilde{M}_p , that is the sum of the planet and circumplanetary disc masses. Related to this point, we comment that the planet and its circumplanetary disc migrate at the same drift rate. When its self-gravity is included, the protoplanetary disc torques both the planet and the circumplanetary disc. However, if self-gravity is discarded, as is usually the case in numerical simulations, the protoplanetary disc can only torque the planet, and the circumplanetary disc remains a passive spectator of the migration. In this case, the planet must exert an additional effort to maintain the planet and circumplanetary disc joint migration. Put another way, the circumplanetary disc artificially slows down migration when self-gravity is discarded. To avoid this artificial slowdown, [15] showed that, in simulations discarding self-gravity, the calculation of the torque on the planet must exclude the material inside the circumplanetary disc. In addition, migration rates with and without self-gravity can be in close agreement, provided that the mass of the circumplanetary disc is added to that of the planet when calculating the gravitational potential felt by the protoplanetary disc.

In the early stages of their formation and orbital evolution, most massive gap-opening planets should be subject to disc-dominated type II migration, and migrate on a timescale comparable to the disc's viscous timescale. Note from Eq. (38) that

this corresponds to the shortest migration timescale a gap-opening planet can get. Depletion of the protoplanetary disc, or substantial migration towards the central object, should, however, slow down migration as the planet's inertial mass becomes comparable to the local disc mass. It is nonetheless interesting to note from Eq. (39) that in the early stages of the disc evolution, type II migration can be relatively fast in the disc's turbulent parts. This may make difficult the maintenance of massive planets at reasonably large orbital separations from their host star. Additional mechanisms, like the effect of stellar irradiation on the disc's density and temperature profiles near the planet's orbit (formation of shadow regions near the gap's inner edge, and irradiated 'puffed up' regions near the gap's outer edge) [40] could help slow down type II migration.

Gap formation and type II migration are intimately related to the disc viscosity in laminar viscous disc models, and a few studies have investigated their properties in MHD turbulent discs [81, 110, 91]. These studies have considered three-dimensional magnetised disc models, where vertical stratification and non-ideal MHD effects were discarded for simplicity. They found that the structure of the annular gap opened by a massive planet in fully MHD turbulent discs is essentially in line with the predictions of viscous disc models with a similar alpha viscous parameter near the planet location. Gaps in turbulent discs tend, however, to be wider than in viscous discs [81, 110]. Some other differences arise between turbulent and viscous disc models, particularly in the vicinity of the planet, where magnetic field lines are compressed and ordered at the location of the wakes and the circumplanetary disc. The connection between the circumplanetary and protoplanetary discs through magnetic field lines can cause magnetic braking of the circumplanetary material [91], which may help increase gas accretion onto the planet [110, 91].

Before leaving this section, we comment that the overall properties of planet–disc interactions with gap-opening planets remain essentially unchanged when taking the disc's vertical stratification into account, and therefore the two-dimensional approximation is valid. Nonetheless, different structures in the flow circulating around the planet in two- and three-dimensions, and the related accretion rate onto the planet, may affect the planet's migration rate (see e.g., [20]).

We summarise the results described in this section:

- Planets massive enough to open a wide and deep annular gap around their orbit are subject to Type II migration.
- When the local disc mass (roughly speaking, the mass interior to the planet orbit) remains large compared to the planet mass, the planet migration timescale corresponds to the viscous drift timescale (disc-dominated type II migration).
- When the planet mass becomes comparable to, or exceeds the local disc mass, migration is slowed down by the planet's inertia (transition to planet-dominated type II migration).

5 Planet migration theories and exoplanets' observed diversity

The properties of planet–disc interactions have been examined in details in the previous sections, with a particular emphasis on the expected migration rate for planets with different masses. The migration rate is intimately related to the disc's physical properties (e.g., mass, sound speed, cooling properties, turbulent stresses) near the planet location, which underlines that the modelling of protoplanetary discs plays as much of an important role as planet–disc interaction theories in predicting the evolution of planetary systems. We continue our exposition with a brief discussion of several aspects of planet–disc interactions which could account for the observed diversity of (extrasolar) planets.

5.1 *Massive planets at large orbital separations*

Amongst the recent discoveries of exoplanets, particularly exciting is the observation by direct imaging of about 10 massive exoplanets located at separations ranging from 10 to 200 AU from their host star (e.g., [61, 47]). Most of these planets are so far observed to be the only planetary companions of their host star. Yet, it is possible that their present location results from a scattering event with another massive companion on a shorter-period orbit. A remarkable exception is the HR 8799 planetary system. It comprises four planets with masses evaluated in the range [7 – 10] Jupiter masses, and estimated separations of 14, 24, 38 and 68 AU [62]. The planets are close to being in mutual mean-motion resonances, and it seems likely that planet–disc interactions could have played a major role in shaping this planetary system. We discuss below the relevance of planet–disc interactions to account for massive planets at large orbital separations.

5.1.1 **Outward migration of a pair of massive resonant planets**

In the standard core-accretion scenario for planet formation, it is difficult to form Jupiter-like planets in isolation further than ~ 10 AU from a Sun-like star [97, 37]. As we have seen in § 4, planets in the Jupiter-mass range orbiting Solar-type stars are expected to open an annular gap around their orbit. If a partial gap is opened, outward runaway type III migration could occur under some circumstances, but as we have discussed in § 4.2, numerical simulations indicate that it is difficult to sustain this outward migration in the long term. If the planet opens a deep gap, inward type II migration is expected. It is therefore unlikely that a single massive planet formed through the core-accretion scenario within ~ 10 AU of its host star could migrate to several tens of AUs.

A notable exception to this generally expected trend has been recently proposed by [16], based on a migration mechanism originally studied by [63]. This mechanism relies on the joint migration of a pair of resonant massive planets embedded

in a common gap. In this mechanism, the innermost planet is massive enough to open a deep gap and migrate inwards on a timescale comparable to that of type II migration. The outermost, less massive planet migrates inwards at a larger pace while carving a partial gap around its orbit. If both planets open overlapping gaps, and maintain a mean-motion resonance between their orbits, their joint migration *could* proceed outwards. The global picture is the following: as the inner planet is more massive, the torque it experiences from the inner disc (inner Lindblad torque) is larger than the (absolute value of the) torque the outer planet experiences from the outer disc (outer Lindblad torque). To maintain joint outward migration in the long term, the fluid elements outside the common gap must be funnelled to the inner disc by embarking on horseshoe trajectories. Otherwise, material would pile up at the outer edge of the common gap, much like a snow-plough, and the torque balance as well as the sense of migration would eventually reverse. An illustration of the joint outward migration mechanism is shown in Fig. 17.

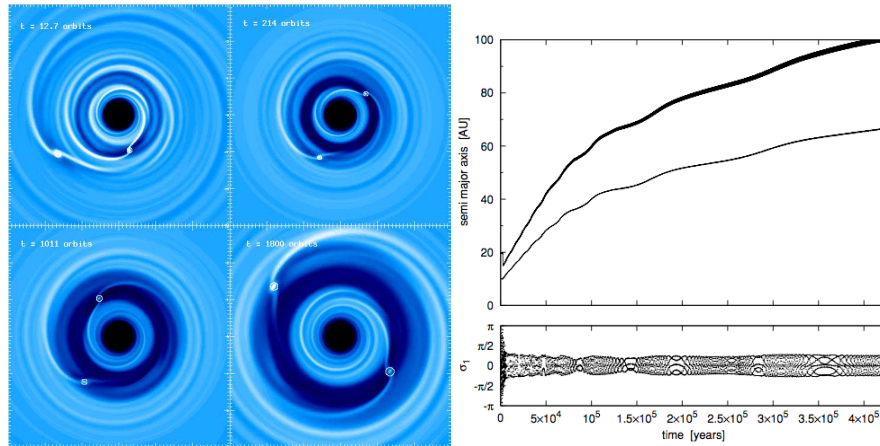


Fig. 17 Illustration of the joint outward migration of a pair of resonant massive planets. The left panel shows the evolution of the disc's surface density perturbed by a Jupiter-mass planet (inner planet) and a Saturn-mass planet (outer one). After an episode of rapid convergent migration (top-left quadrant) resulting in their capture into mean-motion resonance, planets open overlapping gaps (top-right quadrant), which leads to their joint outward migration (lower quadrants). The right panels illustrate the outcome of the same mechanism applied to an inner 3-Jupiter mass planet, and an outer 2-Jupiter-mass planet orbiting a $2M_{\odot}$ mass star (taken from [16]). The time evolution of the planets semi-major axis is shown in the top-right panel, and that of their 2 : 1 critical resonance angle is in the bottom-right panel.

The migration reversal described above requires an asymmetric density profile within the common gap. It is thus sensitive to the disc's aspect ratio and viscosity, which enter the gap-opening criterion. It is also sensitive to the mass ratio of the two planets. If the outer-to-inner planets mass ratio is too small, the density contrast within the common gap will be too large to affect the evolution of the innermost planet (the gas density near the outer planet's orbit remains too large to signifi-

cantly decrease the outer Lindblad torque acting on the inner planet). Conversely, if the outer-to-inner planets mass ratio is too large, the Lindblad torques imbalance will favour joint inward migration. By changing the planets mass ratio during joint migration, gas accretion onto the planets could affect the possibility of sustaining outward migration in the long term. This issue requires further investigation, and accurate modelling of the gas accretion processes onto Saturn sized planets.

We also mention that the joint outward migration scenario has been recently discussed in the context of the Solar System [105]. Inward migration of Jupiter in the primordial Solar nebula down to ≈ 1.5 AU, followed by joint outward migration with Saturn to the current location of both planets (the "Grand tack") would truncate the disc of planetesimals interior to Jupiter's orbit at about 1 AU. The subsequent formation of the terrestrial planets is found to occur with the correct mass ratio between Earth and Mars, and would also account for the compositional structure of the asteroid belt [105].

5.1.2 Migration of planets formed by gravitational instability

An alternative to the core-accretion formation scenario involves the fragmentation of massive protoplanetary discs into clumps through the gravitational instability. Gravitational instability (GI) may typically occur at separations larger than 30 to 50 AU from a central (Sun-like) star, if the Toomre- Q parameter approaches unity and the disc's cooling timescale becomes of order the dynamical timescale (e.g., [98, 29]). While several massive planets could form by fragmentation of a massive disc at several tens of AUs from their star, they are unlikely to stay in place. The tidal interaction with the gravito-turbulent disc they are embedded in should rapidly bring planets formed by GI to the disc's inner regions [11, 75, 113], in a timescale comparable to that of type I migration [11]. The orbital evolution of a single Jupiter-mass planet embedded in a gravito-turbulent disc (where the planet is supposed to have formed by GI) is illustrated in Fig. 18, where we see that the planet migrates from 100 to 20 AU in typically less than 10^4 yrs.

Investigation is under way to determine the evolution of planets formed by GI when they reach the inner parts of protoplanetary discs. The latter should be too hot to be gravitationally unstable, and other sources of turbulence, such as the magnetorotational instability, could prevail, changing the background disc profiles as well as the amount of turbulence. It is thus possible that the rapid type I migration of planets formed by GI slows down in the disc inner parts and results in the formation of a gap. Gap-opening may also occur if significant gas accretion occurs during the planets fast inward migration [113]. Planet–planet interactions, which may result in scattering events, mergers or captures in resonance, should also play a prominent role in shaping planetary systems formed by GI.

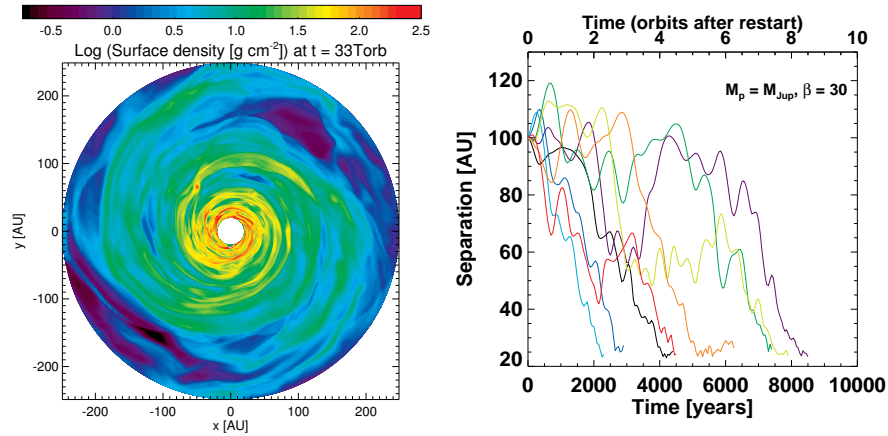


Fig. 18 Jupiter-mass planet embedded in a gravito-turbulent disc. After setting up a quasi steady-state gravito-turbulent disc with (gravito-turbulent) shock heating balancing disc cooling (parametrised here by a simple β -cooling function, see [11]), simulations were restarted with inserting a Jupiter-mass planet at 100 AU. The left panel shows the disc’s surface density three orbits after restart, the planet being located at $x \sim -50$ AU, $y \sim 60$ AU. The right panel displays the time evolution of the planet’s orbital separation in 8 different restart simulations with varying the azimuth of the planet prior to its insertion in the disc. Taken from [11].

5.2 Planet population syntheses

Planetary astrophysics is undergoing an epoch of explosive growth, driven by the observational discoveries of more than 750 exoplanets over the past two decades. Outstanding progress in detection techniques have uncovered planetary systems very different from ours. Since the discovery of the first Hot Jupiter [73], radial velocity surveys have made possible the detection of Earth-like planets, some in the habitable zone of their star [92]. Transit space missions CoRoT and KEPLER are digging out hundreds of close-in extrasolar planets, some in exotic environments (like Kepler-16 b, the first circumbinary exoplanet discovered [26]). Direct imaging has revealed the existence of massive giant planets located at several tens of AU from their star.

Such diversity provides an exciting opportunity to test our theories for the formation and evolution of planetary systems. By coupling theoretical models of planet formation and migration, and of disc evolution, planet population syntheses estimate the statistical distribution of exoplanets according to their mass, semi-major axis, and eccentricity, which they compare to observed distributions [37, 38, 76, 99, 35]. At the moment, models of planet population syntheses are not able to reproduce the statistical properties of extrasolar planets. For instance, they predict a deficit of super-Earths and Neptune-like planets with orbital periods less than 50 days, while observations have revealed a significant number of exoplanets in this range of mass and period [36]. The origin for this discrepancy can be found in uncertain prescriptions for the minimum core mass for the onset of gas accretion [35], as well as in

the modeling of type I migration. The difficulty raised by the excessively rapid inward type I migration, predicted by the long-time reference torque formula by [102], was circumvented by introducing a reduction factor in front of this torque formula. Population syntheses models tried to constrain this factor to reproduce the statistical properties of detected exoplanets. This reduction factor was found to range from 0.01 to 0.1. We note however that the introduction of this reduction factor to provide planetary population synthesis in agreement with the statistics of detected extrasolar planets is *ad hoc*, and that there is no reason to expect that the type I migration drift rates are systematically overestimated in theoretical studies by a factor 10 to 100. Rather, as we emphasized throughout this manuscript, type I migration is very sensitive to the disc’s density and temperature profiles near the planet orbit. Large slopes of mass density and/or temperature, over a limited radial range, may reverse the tidal torque exerted on the planet. This, in turn, may create “planetary traps” at the points where the tidal torque cancels out (much like what was contemplated by [71] for the case of a positive surface density gradient), which can stop incoming protoplanets, depending on their mass. The number and location of these traps may vary as the disc evolves. This view of type I migrating objects subject to several traps on their way to the star [60, 34] sounds more compatible with the state of migration theories than an *ad hoc* reduction factor. This has motivated recent works to produce accurate, yet simple formulae for type I migration [69, 85, 67]. These formulae include a description of the corotation torque in discs with arbitrary viscosity and thermal diffusion, and corrections to the Lindblad torque for discs with non power-law profiles. Their incorporation into models of planet population synthesis will hopefully provide a better comprehension of the diversity of observed exoplanets.

6 Conclusions

We have reviewed the recent progress made in understanding planet–disc interactions, and the resulting planets’ orbital migration. We have particularly focused on the migration of growing protoplanets (type I migration), which has been the subject of intensive investigation over the past five years. Being for a while the second-place actor of planet migration theories, the corotation torque has been shown to play a prominent role in realistic protoplanetary discs, where it can slow down, stall, or reverse type I migration. This review is especially aimed at giving a comprehensive, detailed description of the mechanisms responsible for the corotation torque. The type II and type III migration regimes for gap-opening planets are also reviewed and discussed in the context of observed exoplanets. Being aimed at migration of planets on circular orbits, this review has set aside interesting recent developments on the tidal interactions of eccentric or inclined planets with their discs. We have also focused essentially on the mechanisms that drive the migration of a single planet in a disc, and we have therefore excluded most results about the migration of several planets. For a recent review covering these topics, the reader is referred to [45].

This list of restrictions of the present review stresses that the research on planet–disc interactions is a very active branch of planet formation, with a growing body of avenues. We finally reiterate the plea made in the introduction: planetary migration is not overrated. The tremendous value of each of the tidal torque components exerted on a given planet, associated to the great sensitivity of these torques to the underlying disc structure, appeals for a detailed knowledge of the properties of protoplanetary discs, and significant efforts toward an accurate determination of each torque component. This also reasserts tidal interactions as a prominent process in shaping forming planetary systems.

Acknowledgments

It is a pleasure to thank Jérôme Guilet, Sijme-Jan Paardekooper, and Stephen Thomson for their detailed reading of this manuscript, as well as John Papaloizou for stimulating discussions.

References

1. Artymowicz, P.: Disk-Satellite Interaction via Density Waves and the Eccentricity Evolution of Bodies Embedded in Disks. *ApJ***419**, 166–+ (1993). DOI 10.1086/173470
2. Artymowicz, P.: On the Wave Excitation and a Generalized Torque Formula for Lindblad Resonances Excited by External Potential. *ApJ***419**, 155–+ (1993). DOI 10.1086/173469
3. Ayliffe, B.A., Bate, M.R.: Migration of protoplanets with surfaces through discs with steep temperature gradients. *MNRAS***415**, 576–586 (2011). DOI 10.1111/j.1365-2966.2011.18730.x
4. Balbus, S.A., Hawley, J.F.: A powerful local shear instability in weakly magnetized disks. I - Linear analysis. II - Nonlinear evolution. *ApJ***376**, 214–233 (1991). DOI 10.1086/170270
5. Balmforth, N.J., Korycansky, D.G.: Non-linear dynamics of the corotation torque. *MNRAS***326**, 833–851 (2001). DOI 10.1046/j.1365-8711.2001.04619.x
6. Baruteau, C.: Toward predictive scenarios of planetary migration. Ph.D. thesis, CEA Saclay, Service d’Astrophysique, 91191 Gif/Yvette Cedex, France (2008)
7. Baruteau, C., Fromang, S., Nelson, R.P., Masset, F.: Corotation torques experienced by planets embedded in weakly magnetized turbulent discs. *A&A***533**, A84 (2011). DOI 10.1051/0004-6361/201117227
8. Baruteau, C., Lin, D.N.C.: Protoplanetary Migration in Turbulent Isothermal Disks. *ApJ***709**, 759–773 (2010). DOI 10.1088/0004-637X/709/2/759
9. Baruteau, C., Masset, F.: On the Corotation Torque in a Radiatively Inefficient Disk. *ApJ***672**, 1054–1067 (2008). DOI 10.1086/523667
10. Baruteau, C., Masset, F.: Type I Planetary Migration in a Self-Gravitating Disk. *ApJ***678**, 483–497 (2008). DOI 10.1086/529487
11. Baruteau, C., Meru, F., Paardekooper, S.J.: Rapid inward migration of planets formed by gravitational instability. *MNRAS***416**, 1971–1982 (2011). DOI 10.1111/j.1365-2966.2011.19172.x
12. Bate, M.R., Lubow, S.H., Ogilvie, G.I., Miller, K.A.: Three-dimensional calculations of high- and low-mass planets embedded in protoplanetary discs. *MNRAS***341**, 213–229 (2003). DOI 10.1046/j.1365-8711.2003.06406.x

13. Bryden, G., Chen, X., Lin, D.N.C., Nelson, R.P., Papaloizou, J.C.B.: Tidally Induced Gap Formation in Protostellar Disks: Gap Clearing and Suppression of Protoplanetary Growth. *ApJ***514**, 344–367 (1999). DOI 10.1086/306917
14. Casoli, J., Masset, F.S.: On the Horseshoe Drag of a Low-Mass Planet. I. Migration in Isothermal Disks. *ApJ***703**, 845–856 (2009). DOI 10.1088/0004-637X/703/1/845
15. Crida, A., Baruteau, C., Kley, W., Masset, F.: The dynamical role of the circumplanetary disc in planetary migration. *A&A***502**, 679–693 (2009). DOI 10.1051/0004-6361/200811608
16. Crida, A., Masset, F., Morbidelli, A.: Long Range Outward Migration of Giant Planets, with Application to Fomalhaut b. *ApJL***705**, L148–L152 (2009). DOI 10.1088/0004-637X/705/2/L148
17. Crida, A., Morbidelli, A.: Cavity opening by a giant planet in a protoplanetary disc and effects on planetary migration. *MNRAS***377**, 1324–1336 (2007). DOI 10.1111/j.1365-2966.2007.11704.x
18. Crida, A., Morbidelli, A., Masset, F.: On the width and shape of gaps in protoplanetary disks. *Icarus* **181**, 587–604 (2006). DOI 10.1016/j.icarus.2005.10.007
19. Crida, A., Sándor, Z., Kley, W.: Influence of an inner disc on the orbital evolution of massive planets migrating in resonance. *A&A***483**, 325–337 (2008). DOI 10.1051/0004-6361:20079291
20. D’Angelo, G., Bate, M.R., Lubow, S.H.: The dependence of protoplanet migration rates on co-orbital torques. *MNRAS***358**, 316–332 (2005). DOI 10.1111/j.1365-2966.2005.08866.x
21. D’Angelo, G., Henning, T., Kley, W.: Nested-grid calculations of disk-planet interaction. *A&A***385**, 647–670 (2002)
22. D’Angelo, G., Henning, T., Kley, W.: Thermohydrodynamics of Circumstellar Disks with High-Mass Planets. *ApJ***599**, 548–576 (2003)
23. D’Angelo, G., Kley, W., Henning, T.: Orbital Migration and Mass Accretion of Protoplanets in Three-dimensional Global Computations with Nested Grids. *ApJ***586**, 540–561 (2003)
24. D’Angelo, G., Lubow, S.H.: Evolution of Migrating Planets Undergoing Gas Accretion. *ApJ***685**, 560–583 (2008). DOI 10.1086/590904
25. Dong, R., Rafikov, R.R., Stone, J.M.: Density Waves Excited by Low-mass Planets in Protoplanetary Disks. II. High-resolution Simulations of the Nonlinear Regime. *ApJ***741**, 57 (2011). DOI 10.1088/0004-637X/741/1/57
26. Doyle, L.R., Carter, J.A., Fabrycky, D.C., Slawson, R.W., Howell, S.B., Winn, J.N., Orosz, J.A., Prsa, A., Welsh, W.F., Quinn, S.N., Latham, D., Torres, G., Buchhave, L.A., Marcy, G.W., Fortney, J.J., Shporer, A., Ford, E.B., Lissauer, J.J., Ragozzine, D., Rucker, M., Batalha, N., Jenkins, J.M., Borucki, W.J., Koch, D., Middour, C.K., Hall, J.R., McCauliff, S., Fanelli, M.N., Quintana, E.V., Holman, M.J., Caldwell, D.A., Still, M., Stefanik, R.P., Brown, W.R., Esquerdo, G.A., Tang, S., Furesz, G., Geary, J.C., Berlind, P., Calkins, M.L., Short, D.R., Steffen, J.H., Sasselov, D., Dunham, E.W., Cochran, W.D., Boss, A., Haas, M.R., Buzasi, D., Fischer, D.: Kepler-16: A Transiting Circumbinary Planet. *Science* **333**, 1602–(2011). DOI 10.1126/science.1210923
27. Fleming, T., Stone, J.M.: Local Magnetohydrodynamic Models of Layered Accretion Disks. *ApJ***585**, 908–920 (2003). DOI 10.1086/345848
28. Fromang, S., Terquem, C., Nelson, R.P.: Numerical simulations of type I planetary migration in non-turbulent magnetized discs. *MNRAS***363**, 943–953 (2005). DOI 10.1111/j.1365-2966.2005.09498.x
29. Gammie, C.F.: Nonlinear Outcome of Gravitational Instability in Cooling, Gaseous Disks. *ApJ***553**, 174–183 (2001). DOI 10.1086/320631
30. Gautier III, T.N., Charbonneau, D., Rowe, J.F., Marcy, G.W., Isaacson, H., Torres, G., Fressin, F., Rogers, L.A., Désert, J.M., Buchhave, L.A., Latham, D.W., Quinn, S.N., Ciardi, D.R., Fabrycky, D.C., Ford, E.B., Gilliland, R.L., Walkowicz, L.M., Bryson, S.T., Cochran, W.D., Endl, M., Fischer, D.A., Howel, S.B., Horch, E.P., Barclay, T., Batalha, N., Borucki, W.J., Christiansen, J.L., Geary, J.C., Henze, C.E., Holman, M.J., Ibrahim, K., Jenkins, J.M., Kinemuchi, K., Koch, D.G., Lissauer, J.J., Sanderfer, D.T., Sasselov, D.D., Seager, S., Silverio, K., Smith, J.C., Still, M., Stumpe, M.C., Tenenbaum, P., Van Cleve, J.: Kepler-20: A

- Sun-like Star with Three Sub-Neptune Exoplanets and Two Earth-size Candidates. ArXiv e-prints (2011)
31. Goldreich, P., Tremaine, S.: The excitation of density waves at the Lindblad and corotation resonances by an external potential. *ApJ***233**, 857–871 (1979). DOI 10.1086/157448
 32. Goldreich, P., Tremaine, S.: Disk-satellite interactions. *ApJ***241**, 425–441 (1980). DOI 10.1086/158356
 33. Goodman, J., Rafikov, R.R.: Planetary Torques as the Viscosity of Protoplanetary Disks. *ApJ***552**, 793–802 (2001)
 34. Hasegawa, Y., Pudritz, R.E.: Dead Zones as Thermal Barriers to Rapid Planetary Migration in Protoplanetary Disks. *ApJL***710**, L167–L171 (2010). DOI 10.1088/2041-8205/710/2/L167
 35. Hellary, P., Nelson, R.P.: Global models of planetary system formation in radiatively-inefficient protoplanetary discs. *MNRAS***419**, 2737–2757 (2012). DOI 10.1111/j.1365-2966.2011.19815.x
 36. Howard, A.W., Marcy, G.W., Johnson, J.A., Fischer, D.A., Wright, J.T., Isaacson, H., Valenti, J.A., Anderson, J., Lin, D.N.C., Ida, S.: The Occurrence and Mass Distribution of Close-in Super-Earths, Neptunes, and Jupiters. *Science* **330**, 653– (2010). DOI 10.1126/science.1194854
 37. Ida, S., Lin, D.N.C.: Toward a Deterministic Model of Planetary Formation. I. A Desert in the Mass and Semimajor Axis Distributions of Extrasolar Planets. *ApJ***604**, 388–413 (2004). DOI 10.1086/381724
 38. Ida, S., Lin, D.N.C.: Toward a Deterministic Model of Planetary Formation. IV. Effects of Type I Migration. *ApJ***673**, 487–501 (2008). DOI 10.1086/523754
 39. Ivanov, P.B., Papaloizou, J.C.B., Polnarev, A.G.: The evolution of a supermassive binary caused by an accretion disc. *MNRAS***307**, 79–90 (1999). DOI 10.1046/j.1365-8711.1999.02623.x
 40. Jang-Condell, H.: Planet Shadows in Protoplanetary Disks. I. Temperature Perturbations. *ApJ***679**, 797–812 (2008). DOI 10.1086/533583
 41. Johansen, A., Henning, T., Klahr, H.: Dust Sedimentation and Self-sustained Kelvin-Helmholtz Turbulence in Protoplanetary Disk Midplanes. *ApJ***643**, 1219–1232 (2006). DOI 10.1086/502968
 42. Klahr, H.H., Bodenheimer, P.: Turbulence in Accretion Disks: Vorticity Generation and Angular Momentum Transport via the Global Baroclinic Instability. *ApJ***582**, 869–892 (2003)
 43. Kley, W., Bitsch, B., Klahr, H.: Planet migration in three-dimensional radiative discs. *A&A***506**, 971–987 (2009). DOI 10.1051/0004-6361/200912072
 44. Kley, W., Crida, A.: Migration of protoplanets in radiative discs. *A&A***487**, L9–L12 (2008). DOI 10.1051/0004-6361:200810033
 45. Kley, W., Nelson, R.P.: Planet-disk interaction and orbital evolution. ArXiv e-prints (2012)
 46. Korycansky, D.G., Pollack, J.B.: Numerical calculations of the linear response of a gaseous disk to a protoplanet. *Icarus* **102**, 150–165 (1993). DOI 10.1006/icar.1993.1039
 47. Lagrange, A., Bonnefoy, M., Chauvin, G., Apai, D., Ehrenreich, D., Boccaletti, A., Gratadour, D., Rouan, D., Mouillet, D., Lacour, S., Kasper, M.: A Giant Planet Imaged in the Disk of the Young Star β Pictoris. *Science* **329**, 57– (2010). DOI 10.1126/science.1187187
 48. Laughlin, G., Steinacker, A., Adams, F.C.: Type I Planetary Migration with MHD Turbulence. *ApJ***608**, 489–496 (2004). DOI 10.1086/386316
 49. Lesur, G., Papaloizou, J.C.B.: The subcritical baroclinic instability in local accretion disc models. *A&A***513**, A60 (2010). DOI 10.1051/0004-6361/200913594
 50. Li, H., Finn, J.M., Lovelace, R.V.E., Colgate, S.A.: Rossby Wave Instability of Thin Accretion Disks. II. Detailed Linear Theory. *ApJ***533**, 1023–1034 (2000). DOI 10.1086/308693
 51. Lin, D.N.C., Papaloizou, J.: Tidal torques on accretion discs in binary systems with extreme mass ratios. *MNRAS***186**, 799–812 (1979)
 52. Lin, D.N.C., Papaloizou, J.: On the tidal interaction between protoplanets and the protoplanetary disk. III - Orbital migration of protoplanets. *ApJ***309**, 846–857 (1986). DOI 10.1086/164653
 53. Lin, D.N.C., Papaloizou, J.C.B.: On the tidal interaction between protostellar disks and companions. In: E.H. Levy, J.I. Lunine (eds.) *Protostars and Planets III*, pp. 749–835 (1993)

54. Lin, M.K., Papaloizou, J.C.B.: Type III migration in a low-viscosity disc. *MNRAS***405**, 1473–1490 (2010). DOI 10.1111/j.1365-2966.2010.16560.x
55. Lin, M.K., Papaloizou, J.C.B.: Edge modes in self-gravitating disc-planet interactions. *MNRAS***415**, 1445–1468 (2011). DOI 10.1111/j.1365-2966.2011.18797.x
56. Lin, M.K., Papaloizou, J.C.B.: The effect of self-gravity on vortex instabilities in disc-planet interactions. *MNRAS***415**, 1426–1444 (2011). DOI 10.1111/j.1365-2966.2011.18798.x
57. Lin, M.K., Papaloizou, J.C.B.: Outward migration of a giant planet with a gravitationally unstable gap edge. *MNRAS***421**, 780–788 (2012). DOI 10.1111/j.1365-2966.2011.20352.x
58. Lovelace, R.V.E., Li, H., Colgate, S.A., Nelson, A.F.: Rossby Wave Instability of Keplerian Accretion Disks. *ApJ***513**, 805–810 (1999). DOI 10.1086/306900
59. Lyra, W., Klahr, H.: The baroclinic instability in the context of layered accretion. Self-sustained vortices and their magnetic stability in local compressible unstratified models of protoplanetary disks. *A&A***527**, A138 (2011). DOI 10.1051/0004-6361/201015568
60. Lyra, W., Paardekooper, S.J., Mac Low, M.M.: Orbital Migration of Low-mass Planets in Evolutionary Radiative Models: Avoiding Catastrophic Infall. *ApJL***715**, L68–L73 (2010). DOI 10.1088/2041-8205/715/2/L68
61. Marois, C., Macintosh, B., Barman, T., Zuckerman, B., Song, I., Patience, J., Lafrenière, D., Doyon, R.: Direct Imaging of Multiple Planets Orbiting the Star HR 8799. *Science* **322**, 1348– (2008). DOI 10.1126/science.1166585
62. Marois, C., Zuckerman, B., Konopacky, Q.M., Macintosh, B., Barman, T.: Images of a fourth planet orbiting HR 8799. *Nature***468**, 1080–1083 (2010). DOI 10.1038/nature09684
63. Masset, F., Snellgrove, M.: Reversing type II migration: resonance trapping of a lighter giant protoplanet. *MNRAS***320**, L55+ (2001)
64. Masset, F.S.: On the Co-orbital Corotation Torque in a Viscous Disk and Its Impact on Planetary Migration. *ApJ***558**, 453–462 (2001)
65. Masset, F.S.: The co-orbital corotation torque in a viscous disk: Numerical simulations. *A&A***387**, 605–623 (2002)
66. Masset, F.S.: Planet-Disk Interactions. In: *EAS Publications Series, EAS Publications Series*, vol. 29, pp. 165–244 (2008). DOI 10.1051/eas:0829006
67. Masset, F.S.: On type-I migration near opacity transitions. A generalized Lindblad torque formula for planetary population synthesis. *Celestial Mechanics and Dynamical Astronomy* **111**, 131–160 (2011). DOI 10.1007/s10569-011-9364-0
68. Masset, F.S., Casoli, J.: On the Horseshoe Drag of a Low-Mass Planet. II. Migration in Adiabatic Disks. *ApJ***703**, 857–876 (2009). DOI 10.1088/0004-637X/703/1/857
69. Masset, F.S., Casoli, J.: Saturated Torque Formula for Planetary Migration in Viscous Disks with Thermal Diffusion: Recipe for Protoplanet Population Synthesis. *ApJ***723**, 1393–1417 (2010). DOI 10.1088/0004-637X/723/2/1393
70. Masset, F.S., D’Angelo, G., Kley, W.: On the Migration of Protoplanet Solid Cores. *ApJ***652**, 730–745 (2006). DOI 10.1086/507515
71. Masset, F.S., Morbidelli, A., Crida, A., Ferreira, J.: Disk Surface Density Transitions as Protoplanet Traps. *ApJ***642**, 478–487 (2006). DOI 10.1086/500967
72. Masset, F.S., Papaloizou, J.C.B.: Runaway Migration and the Formation of Hot Jupiters. *ApJ***588**, 494–508 (2003)
73. Mayor, M., Queloz, D.: A Jupiter-Mass Companion to a Solar-Type Star. *Nature***378**, 355– (1995). DOI 10.1038/378355a0
74. Menou, K., Goodman, J.: Low-Mass Protoplanet Migration in T Tauri α -Disks. *ApJ***606**, 520–531 (2004). DOI 10.1086/382947
75. Michael, S., Durisen, R.H., Boley, A.C.: Migration of Gas Giant Planets in Gravitationally Unstable Disks. *ApJL***737**, L42 (2011). DOI 10.1088/2041-8205/737/2/L42
76. Mordasini, C., Alibert, Y., Benz, W., Naef, D.: Extrasolar planet population synthesis. II. Statistical comparison with observations. *A&A***501**, 1161–1184 (2009). DOI 10.1051/0004-6361/200810697
77. Morohoshi, K., Tanaka, H.: Gravitational interaction between a planet and an optically thin disc. *MNRAS***346**, 915–923 (2003). DOI 10.1111/j.1365-2966.2003.07140.x

78. Murray, C.D., Dermott, S.F.: *Solar System Dynamics*. Solar System Dynamics, by C.D. Murray and S.F. Dermott. ISBN 0521575974. Cambridge, UK: Cambridge University Press, 2000. (2000)
79. Muto, T., Machida, M.N., Inutsuka, S.i.: The Effect of Poloidal Magnetic Field on Type I Planetary Migration: Significance of Magnetic Resonance. *ApJ***679**, 813–826 (2008). DOI 10.1086/587027
80. Nelson, R.P.: On the orbital evolution of low mass protoplanets in turbulent, magnetised disks. *A&A***443**, 1067–1085 (2005). DOI 10.1051/0004-6361:20042605
81. Nelson, R.P., Papaloizou, J.C.B.: The interaction of a giant planet with a disc with MHD turbulence - II. The interaction of the planet with the disc. *MNRAS***339**, 993–1005 (2003). DOI 10.1046/j.1365-8711.2003.06247.x
82. Nelson, R.P., Papaloizou, J.C.B.: The interaction of giant planets with a disc with MHD turbulence - IV. Migration rates of embedded protoplanets. *MNRAS***350**, 849–864 (2004). DOI 10.1111/j.1365-2966.2004.07406.x
83. Ogilvie, G.I., Lubow, S.H.: On the wake generated by a planet in a disc. *MNRAS***330**, 950–954 (2002). DOI 10.1046/j.1365-8711.2002.05148.x
84. Paardekooper, S., Baruteau, C., Crida, A., Kley, W.: A torque formula for non-isothermal type I planetary migration - I. Unsaturated horseshoe drag. *MNRAS***401**, 1950–1964 (2010). DOI 10.1111/j.1365-2966.2009.15782.x
85. Paardekooper, S., Baruteau, C., Kley, W.: A torque formula for non-isothermal Type I planetary migration - II. Effects of diffusion. *MNRAS***410**, 293–303 (2011). DOI 10.1111/j.1365-2966.2010.17442.x
86. Paardekooper, S.J., Mellema, G.: Halting type I planet migration in non-isothermal disks. *A&A***459**, L17–L20 (2006). DOI 10.1051/0004-6361:20066304
87. Paardekooper, S.J., Mellema, G.: Growing and moving low-mass planets in non-isothermal disks. *A&A***478**, 245–266 (2008). DOI 10.1051/0004-6361:20078592
88. Paardekooper, S.J., Papaloizou, J.C.B.: On disc protoplanet interactions in a non-barotropic disc with thermal diffusion. *A&A***485**, 877–895 (2008). DOI 10.1051/0004-6361:20078702
89. Paardekooper, S.J., Papaloizou, J.C.B.: On corotation torques, horseshoe drag and the possibility of sustained stalled or outward protoplanetary migration. *MNRAS***394**, 2283–2296 (2009). DOI 10.1111/j.1365-2966.2009.14511.x
90. Paardekooper, S.J., Papaloizou, J.C.B.: On the width and shape of the corotation region for low-mass planets. *MNRAS***394**, 2297–2309 (2009). DOI 10.1111/j.1365-2966.2009.14512.x
91. Papaloizou, J.C.B., Nelson, R.P., Snellgrove, M.D.: The interaction of giant planets with a disc with MHD turbulence - III. Flow morphology and conditions for gap formation in local and global simulations. *MNRAS***350**, 829–848 (2004). DOI 10.1111/j.1365-2966.2004.07566.x
92. Pepe, F., Lovis, C., Ségransan, D., Benz, W., Bouchy, F., Dumusque, X., Mayor, M., Queloz, D., Santos, N.C., Udry, S.: The HARPS search for Earth-like planets in the habitable zone. I. Very low-mass planets around μ ASTROBJ₁/HD 20794₁/ASTROBJ₁, μ ASTROBJ₂/HD 85512₂/ASTROBJ₂, and μ ASTROBJ₃/HD 192310₃/ASTROBJ₃. *A&A***534**, A58 (2011). DOI 10.1051/0004-6361/201117055
93. Pepliński, A., Artymowicz, P., Mellema, G.: Numerical simulations of type III planetary migration - I. Disc model and convergence tests. *MNRAS***386**, 164–178 (2008). DOI 10.1111/j.1365-2966.2008.13045.x
94. Pepliński, A., Artymowicz, P., Mellema, G.: Numerical simulations of type III planetary migration - II. Inward migration of massive planets. *MNRAS***386**, 179–198 (2008). DOI 10.1111/j.1365-2966.2008.13046.x
95. Pepliński, A., Artymowicz, P., Mellema, G.: Numerical simulations of type III planetary migration - III. Outward migration of massive planets. *MNRAS***387**, 1063–1079 (2008). DOI 10.1111/j.1365-2966.2008.13339.x
96. Pierens, A., Huré, J.M.: How does disk gravity really influence type-I migration? *A&A***433**, L37–L40 (2005). DOI 10.1051/0004-6361:200500099

97. Pollack, J.B., Hubickyj, O., Bodenheimer, P., Lissauer, J.J., Podolak, M., Greenzweig, Y.: Formation of the Giant Planets by Concurrent Accretion of Solids and Gas. *Icarus* **124**, 62–85 (1996). DOI 10.1006/icar.1996.0190
98. Rafikov, R.R.: Can Giant Planets Form by Direct Gravitational Instability? *ApJL* **621**, L69–L72 (2005). DOI 10.1086/428899
99. Schlaufman, K.C., Lin, D.N.C., Ida, S.: The Signature of the Ice Line and Modest Type I Migration in the Observed Exoplanet Mass-Semimajor Axis Distribution. *ApJ* **691**, 1322–1327 (2009). DOI 10.1088/0004-637X/691/2/1322
100. Shakura, N.I., Sunyaev, R.A.: Black holes in binary systems. Observational appearance. *A&A* **24**, 337–355 (1973)
101. Syer, D., Clarke, C.J.: Satellites in discs: regulating the accretion luminosity. *MNRAS* **277**, 758–766 (1995)
102. Tanaka, H., Takeuchi, T., Ward, W.R.: Three-Dimensional Interaction between a Planet and an Isothermal Gaseous Disk. I. Corotation and Lindblad Torques and Planet Migration. *ApJ* **565**, 1257–1274 (2002)
103. Terquem, C.E.J.M.L.J.: Stopping inward planetary migration by a toroidal magnetic field. *MNRAS* **341**, 1157–1173 (2003). DOI 10.1046/j.1365-8711.2003.06455.x
104. Uribe, A.L., Klahr, H., Flock, M., Henning, T.: Three-dimensional Magnetohydrodynamic Simulations of Planet Migration in Turbulent Stratified Disks. *ApJ* **736**, 85 (2011). DOI 10.1088/0004-637X/736/2/85
105. Walsh, K.J., Morbidelli, A., Raymond, S.N., O’Brien, D.P., Mandell, A.M.: A low mass for Mars from Jupiter’s early gas-driven migration. *Nature* **475**, 206–209 (2011). DOI 10.1038/nature10201
106. Ward, W.R.: Density waves in the solar nebula - Differential Lindblad torque. *Icarus* **67**, 164–180 (1986). DOI 10.1016/0019-1035(86)90182-X
107. Ward, W.R.: Horseshoe Orbit Drag. In: Lunar and Planetary Institute Conference Abstracts, pp. 1463–+ (1991)
108. Ward, W.R.: Protoplanet Migration by Nebula Tides. *Icarus* **126**, 261–281 (1997)
109. Ward, W.R.: A Streamline Model of Horseshoe Torque Saturation. In: Lunar and Planetary Institute Science Conference Abstracts, *Lunar and Planetary Institute Science Conference Abstracts*, vol. 38, p. 2289 (2007)
110. Winters, W.F., Balbus, S.A., Hawley, J.F.: Gap Formation by Planets in Turbulent Protostellar Disks. *ApJ* **589**, 543–555 (2003). DOI 10.1086/374409
111. Zhang, H., Lai, D.: Wave excitation in three-dimensional discs by external potential. *MNRAS* **368**, 917–934 (2006). DOI 10.1111/j.1365-2966.2006.10167.x
112. Zhang, H., Yuan, C., Lin, D.N.C., Yen, D.C.C.: On the Orbital Evolution of a Jovian Planet Embedded in a Self-Gravitating Disk. *ApJ* **676**, 639–650 (2008). DOI 10.1086/528707
113. Zhu, Z., Hartmann, L., Nelson, R.P., Gammie, C.F.: Challenges in Forming Planets by Gravitational Instability: Disk Irradiation and Clump Migration, Accretion, and Tidal Destruction. *ApJ* **746**, 110 (2012). DOI 10.1088/0004-637X/746/1/110